Further evidence for natal kick segregation by spectral type in high-mass X-ray binaries

Pornisara Nuchvanichakul,[1,2]* Poshak Gandhi,[2] Christian Knigge,[2] Yue Zhao,[2]
Puji Irawati,[3] Suwicha Wanawichian[1,3] and Cordelia Dashwood Brown[2]

[1]*Department of Physics and Materials Science, Faculty of Science, Chiang Mai University, Chiang Mai, Thailand 50200*
[2]*Department of Physics and Astronomy, University of Southampton, Highfield, Southampton SO17 1BJ, UK*
[3]*National Astronomical Research Institute of Thailand, Chiang Mai, Thailand 50180*

ABSTRACT

High-mass X-ray binaries (HMXBs) are systems in which a neutron star or black hole accretes material from a massive companion. HMXBs are expected to have experienced a supernova in their evolution. The impulsive kick associated with this event should affect the space velocity of the system in a way that depends on the nature and state of the progenitor binary. Here, we test whether the different evolutionary histories of HMXBs have left a detectable imprint on their peculiar velocities ($V_{\rm pec}$). Using data from *Gaia* Data Release 3 (*Gaia* DR3), we first calculate the $V_{\rm pec}$ values for 63 well-known HMXBs hosting a black hole or neutron star and estimate the associated uncertainties via Monte Carlo re-sampling. We then analyse their distribution and check for differences between classes. Overall, $V_{\rm pec}$ estimates extend up to 100 km s^{-1}, but with Be/X-ray binaries (BeXRBs) favouring $V_{\rm pec} \lesssim 40$ km s^{-1} and supergiant X-ray binaries (SgXRBs) favouring $V_{\rm pec} \gtrsim 40$ km s^{-1}. Based on a Kolmogorov–Smirnov (K-S) test, the null hypothesis that the peculiar velocities of both classes are drawn from the same parent distribution can be robustly rejected, irrespective of the background stellar velocity dispersion. Tests with binary population synthesis demonstrate that SgXRBs typically have shorter orbital periods and higher fractional mass loss than BeXRBs at supernova. We argue that the magnitude of $V_{\rm pec}$ could be used as a complementary feature to distinguish between Be and supergiant systems. These findings extend previous inferences based on two-dimensional kinematics from *Hipparcos*, and may be explained by the differing nature of the respective progenitors systems between the source classes at the instant of supernova.

Key words: parallaxes – stars: kinematics and dynamics – stars: neutron stars – stars: black holes – supernovae: general – X-rays: binaries

1 INTRODUCTION

High-mass X-ray binaries (HMXBs) are mass-exchanging binary systems comprising a massive OB-star gravitationally bound to a compact object, either a neutron star or a black hole. The non-degenerate companions of HMXBs typically have masses in excess of $10\,M_\odot$. As a result, due to their immense brightness, HMXBs are excellent tools for probing Galactic star formation and compact objects. Estimating the total number of HMXB systems in the Milky Way is notoriously difficult due to unknown binary evolution physics. Over a hundred well-characterised HMXBs are currently known (Liu et al. 2006; Bird et al. 2016; Neumann et al. 2023).

Much still remains to be understood regarding the origin of HMXBs. During the supernova explosion, an impulsive kick can be imparted to the compact object. These kicks can have a decisive impact on the subsequent evolution and spatial distribution of HMXBs. Kicks can either be a result of symmetric mass loss (e.g., Blaauw 1961) or of asymmetric ejecta in the supernova explosion (e.g., Chugai 1984; Dorofeev et al. 1985; Arras & Lai 1999; Janka 2017; Renzo et al. 2019). The strength of this 'natal velocity kick'

($V_{\rm nk}$) is thus a key ingredient for Galactic compact object population synthesis models and also for understanding the recent gravitational wave (GW) population (e.g. Dominik et al. 2012). Observationally, there are so far very few constraints on $V_{\rm nk}$, even for the bright HMXB population. One of the best-known cases is the BH-hosting HMXB Cyg X-1, which has been confirmed to have suffered only a very mild kick $V_{\rm nk} \leq 20$ km s^{-1} (e.g., Mirabel 2017). This has allowed the conclusive identification of the Cyg OB3 cluster as the natal site of this system (Rao et al. 2020a).

The low kick velocity inferred for Cyg X-1 is consistent with theoretical models in which kicks are momentum-conserving, i.e. in which $V_{\rm nk}$ scales inversely with black hole mass (at least qualitatively; e.g., Fryer & Kalogera 2001, Gandhi et al. 2019). However, this idea remains somewhat speculative (e.g., Repetto et al. 2017, Atri et al. 2019, Gandhi et al. 2020). A recent study on distinct distribution between high-mass X-ray binaries (HMXBs) and low-mass X-ray binaries (LMXBs) provides empirical evidence of an inverse relationship between systemic velocity with respect to the total binary mass (Zhao et al. 2023), albeit with much scatter.

HMXBs are typically amongst the brightest of the XRB population, as well as the youngest. These factors help to mitigate some of the key uncertainties related to kick inference and their evolution-

---

* E-mail: pornisara.nuchvanichakul@soton.ac.uk

ary consequences, provided that key system parameters can be well constrained. HMXBs can be classified into three sub-classes, based on the nature of the secondary and the mass transfer process. Two of these are the OB-supergiant systems (hereafter SgXRBs) and the Be/X-ray binaries (hereafter BeXRBs). In both of these sub-classes, the binary components are detached. In SgXRBs the compact object accretes from the stellar wind of its massive companion; in BeXRBs accretion mainly takes place during periastron passages, when the compact object passes through the decretion disk surrounding the rapidly rotating Be star (Fornasini et al. 2023).The third sub-class is comprised of semi-detached systems, in which the non-degenerate companion loses mass to the compact object via Roche-lobe overflow (RLO) onto an accretion disc (Negueruela 2010).

Interestingly, previous studies with the *Hipparcos* mission (Chevalier & Ilovaisky 1998) found rather high transverse sky velocities for SgXRBs ($V_t \sim 60$ km s^{-1}and up to 90 km s^{-1}), exceeding those of BeXRBs (average V_t value ~ 11 km s^{-1}). The parameter V_t here is a two-dimensional (2-D) tracer of the three-dimensional (3-D) 'peculiar velocity' (V_{pec}), with both referring to the motion relative to the Galactic rest frame (i.e., in excess of Galactic rotation, under the assumption that the system originated within the Galactic disc). Differences between the space velocities of different HMXB types could be suggestive of distinct evolutionary channels. However, before we can exploit this idea, we first need to confirm and quantify these differences. This is what we aim to undertake here.

Gaia is a key mission of the European Space Agency's (ESA's) science programme, with its design goals relying heavily on astrometric, as well as photometric and spectroscopic surveys. The Third *Gaia* Data Release, known as *Gaia* DR3, published data from approximately 1.8 billion sources (Gaia Collaboration 2016, 2023). For bright and moderately faint sources, *Gaia* provides 5-parameter astrometry, including positions in right ascension (α), declination (δ), proper motions ($\mu_\alpha \cos \delta$, μ_δ), and parallaxes (π), with G-band magnitude ranging over ~ 6 to 21 (Lindegren et al. 2021). Several studies have utilised *Gaia* data to investigate the kinematics and peculiar motions of X-ray binaries (XRBs; cf. Gandhi et al. 2019; Atri et al. 2019; Rao et al. 2020a; Zhao et al. 2023).

The first focused study of HMXB sample kinematics was the aforementioned work by Chevalier & Ilovaisky (1998), who found differences in the kinematics of Sg vs. BeXRBs, but were limited in having access to only *2-D* (tangential) velocities from *Hipparcos* for a small ensemble of 17 systems. Using updated *Gaia* Early Data Release 3 (EDR3) astrometry together with archival radial velocity information, Fortin et al. (2022) extracted 3-D kinematics of 35 *neutron-star* HMXBs, finding a V_{pec} distribution peaking around 116 km s^{-1}. They also found a tendency for SgXRBs to have higher V_{pec} values than BeXRBs but did not statistically quantify this trend.

In this work, we build on previous studies by utilising the latest precise measurements of stellar kinematics provided by the *Gaia* DR3 catalogue (Gaia Collaboration 2023). *Gaia* DR3 offers significant advancements over earlier releases, including updated radial velocities for approximately 34 million sources (compared to about 7 million in DR2/EDR3) and an extensive range of new data, such as detailed astrophysical parameters, quasar (QSO) candidates, solar system object data, and specific object studies (Gaia Collaboration 2023). We include systemic radial velocities (V_r) — either direct measurements where available, or their estimates — in our analysis, allowing us to compute the full 3-D V_{pec} values. We also include key black hole HMXB systems, enabling a more complete view of HMXB kinematics. Collating this sample allows us to test whether the evolutionary histories of the various HMXB classes leave an imprint on their kinematics. In Section 2, we describe the *Gaia*

counterpart search and sample selection process. Section 3 describes the *Gaia* distance estimation methodology. In Section 4, we describe the calculation of peculiar velocities. Section 5 presents the results along with the statistical methods used in our analysis. In Section 6, we discuss our inferred peculiar velocities, the comparison of the two sub-classes, and completeness and selection effects. Finally, in Section 7, we summarise our findings.

2 GAIA COUNTERPART SEARCH AND ASSOCIATION

Our starting parent sample comprises 114 systems selected from the fourth edition of the Liu et al. (2006) HMXB catalogue, 8 additional HMXBs identified by *INTEGRAL* (Bird et al. 2016), plus the XRB MWC 656, which has been suggested to host a BH (Aleksić et al. 2015, but see Section 7.1.1). Additionally, we also included two rare cases of symbiotic X-ray binaries (SyXRBs): 4U 1954+31 and Swift J0850.8–4219 (De et al. 2024). SyXRBs are characterised by the presence of a strongly magnetised neutron star and a late-type companion (Bozzo et al. 2022), and are included because they, like other sub-classes in HMXBs, have experienced a supernova event that formed the compact object. These two systems are the only two confirmed Galactic SyXRBs, and both have astrometric data available. Furthermore, we include Swift J0243.6+6124, BeXRBs recognised as the first Galactic ultraluminous X-ray pulsar (ULXP) (Doroshenko et al. 2018; Tsygankov et al. 2018; Wilson-Hodge et al. 2018), which is not listed in the catalogues mentioned above.

A few sources were discarded from this parent sample. SAX J1819.3–2525, 1WGA J0648.0–4419 and IGR J12349–6434 are not HMXBs in the sense that we adopt in this work. The mass of the companion of SAX J1819.3–2525 is only 2.9 $M_\odot$, making this system an intermediate-mass X-ray binary (IMXB). Similarly, the companion of 1WGA J0648.0–4419 is a hot sub-dwarf (Jaschek & Jaschek 1963), and the optical counterpart of IGR J12349–6434 — RT Cru — has been classified as a symbiotic star which consists of a white dwarf (WD) and a red giant (RG) companion (Luna & Sokoloski 2007; Gromadzki et al. 2013; Ducci et al. 2016). The systems OAO 1657–415, XTE J1543–568, and XTE J1858+034 have no known optical or infrared counterparts. AX J1749.2–2725 has an infrared counterpart, but no optical one and also lies close to a very bright, unrelated star (Karasev et al. 2010). On the other hand, we were able to retain two systems, 4U 1258–61 and IGR J16465–4507, that only have infrared counterparts with relatively large positional uncertainties (2″ and 4″, respectively). We found close matches within 0.37″and 0.16″of their nominal positions, respectively, which we consider as genuine matches. This leaves 110 systems in our final parent sample.

We then queried the *Gaia* DR3 archive for sources within 5″ of the literature positions. This search radius is larger than the positional uncertainty on most (but not all) HMXBs in our parent sample, so some of the queries yielded more than one possible *Gaia* counterpart. In all but two cases, the closest match was within 1″. We carried out checks to ensure the correct counterparts were identified among the *Gaia* sources within the search radius. In particular, the *Gaia* magnitudes and source identifiers were compared to the entries for the target HMXB in both Liu et al. (2006) and relevant archived references in the SIMBAD database.[1] For the four HMXBs where the closest *Gaia* source was located more than 1″ from the nominal position of the target, we carried out additional tests. These HMXBs are

---

[1] http://simbad.u-strasbg.fr/simbad

4U 0115+634, 4U 0352+309, RX J0812.4–3114, and AX 1845.0–0433. For 4U 0115+634, we used the Robotic Optical Transient Experiment (*ROTSE*) observations of its optical counterpart, V635 Cas, to confirm that the closest *Gaia* source is the correct counterpart (Baykal et al. 2005). We also compared its position with the finding chart given by Johnston et al. (1978) and subsequently updated the position based on the optical observations of the HMXBs' companion reported by by Reig & Fabregat (2015). We have chosen to adopt the positional coordinates provided by Reig & Fabregat (2015) as the reference in the literature. The optical counterpart of 4U 0352+309 is the bright variable star X Per, which made it easy to ascertain that the nearest *Gaia* match is the correct counterpart. In the case of RX J0812.4–3114, we cross-check the finding chart and use the X-ray position provided by Motch et al. (1997). For AX 1845.0–0433, a comparison between the finding chart provided by Coe et al. (1996) and the *Gaia* position confirms the accuracy of the source's location. Consequently, we adopt the precise X-ray-based position reported by Coe et al. (1996), which has a positional uncertainty of 0.5″, as the literature position.

All of the 110 *Gaia* counterparts have 5-parameter astrometric solutions in *Gaia* DR3. Distance estimation from parallax is not straightforward when the parallax uncertainty is large. To address this, we discard systems with fractional parallax errors larger than 20% to avoid inaccurate and highly asymmetric error estimates. (c.f. Bailer-Jones 2015). Our final HMXB sample is listed in Table 1 and contains 63 systems, and their photometric and astrometric information is provided in Table 2. These systems exhibited a range of G-band magnitudes between 6 and 14 and were predominantly located in the Galactic plane, with Galactic latitudes ranging from $b = -17.1°$ to $b = 5.7°$.

3 DISTANCE ESTIMATION WITH GAIA

Although *Gaia* provides precision astrometric measurements, these are not free of systematic biases (Lindegren & Bastian 2010). One of the biases impacting the reported parallaxes manifests as a zero-point offset whose size depends on the magnitude, colour, and ecliptic latitude of the source (Lindegren et al. 2021). In order to estimate the parallax zero-point offset values (ZP) for our sources, we used the Python package GAIADR3_ZEROPOINT[2], which implements the corrections described in Lindegren et al. (2021). Following Groenewegen (2021), we then obtain an estimate of the true parallax (π_t) by applying a correction as $\pi_t = \pi_o - ZP$, where π_o is the observed parallax from *Gaia* DR3.

We then use the zero-point-corrected parallaxes to estimate distances. Since all sources in our sample have parallax uncertainties less than 20%, parallax inversion, i.e. $r_{Gaia} = 1/\pi_t$, is a fair estimator of their distances (Bailer-Jones 2015).

[2] https://gitlab.com/icc-ub/public/gaiadr3_zeropoint

Table 1. Basic properties of the HMXB sample. For each source, we provide literature and *Gaia* DR3 coordinates, the offsets between these positions and the *Gaia* G-band magnitude (G).

No.	Source	Type	Literature		Gaia		Offset	G
			α (J2000) (h:m:s)	δ (J2000) (d:m:s)	α (J2015.5) (h:m:s)	δ (J2015.5) (d:m:s)	(″)	mag
1	IGR J00370+6122	Be	00:37:10.00	+61:21:35.0	00:37:09.636	+61:21:36.49	3.03	9.45
2	2S 0114+650	Sg	01:18:02.70	+65:17:30.0	01:18:02.694	+65:17:29.84	0.16	10.52
3	4U 0115+634	Be	01:18:31.80	+63:44:33.0	01:18:31.966	+63:44:33.08	1.11	14.30
4	IGR J01363+6610	Be	01:35:50.00	+66:12:40.0	01:35:49.852	+66:12:43.28	3.40	12.46
5	RX J0146.9+6121	Be	01:47:00.20	+61:21:23.7	01:47:00.212	+61:21:23.66	0.08	11.22
6	IGR J01583+6713	Be	01:58:18.20	+67:13:25.9	01:58:18.491	+67:13:23.46	2.95	13.69
7	1E 0236.6+6100	Be	02:40:31.70	+61:13:46.0	02:40:31.660	+61:13:45.59	0.49	10.40
8	V 0332+53	Be	03:34:59.90	+53:10:24.0	03:34:59.911	+53:10:23.30	0.70	14.20
9	4U 0352+309	Be	03:55:23.10	+31:02:45.0	03:55:23.080	+31:02:45.01	0.31	6.26
10	XTE J0421+560	Sg	04:19:42.20	+55:59:59.0	04:19:42.135	+55:59:57.70	1.41	10.77
11	RX J0440.9+4431	Be	04:40:59.30	+44:31:49.0	04:40:59.330	+44:31:49.24	0.40	10.40
12	EXO 051910+3737.7	Be	05:22:35.20	+37:40:34.0	05:22:35.230	+37:40:33.58	0.58	7.23
13	1A 0535+262	Be	05:38:54.60	+26:18:57.0	05:38:54.570	+26:18:56.79	0.40	8.60
14	1H 0556+286	unclear	05:55:55.10	+28:47:06.0	05:55:55.040	+28:47:06.39	0.86	10.01
15	IGR J06074+2205	Be	06:07:26.60	+22:05:48.3	06:07:26.613	+22:05:47.75	0.58	12.17
16	XTE J0658−073	unclear	06:58:17.30	−07:12:35.3	06:58:17.287	−07:12:35.18	0.22	11.99
17	3A 0726−260	unclear	07 28 53.60	−26 06 29.0	07:28:53.578	−26:06:28.87	0.33	11.60
18	1H 0739−529	unclear	07:47:23.60	−53:19:57.0	07:47:23.580	−53:19:56.69	0.37	7.54
19	RX J0812.4−3114	unclear	08:12:28.40	−31:14:51.0	08:12:28.356	−31:14:52.10	1.24	12.42
20	4U 0900−40	Sg	09:02:06.90	−40:33:17.0	09:02:06.850	−40:33:16.76	0.58	6.74
21	GRO J1008−57	Be	10:09:46.90	−58:17:35.5	10:09:46.955	−58:17:35.55	0.43	13.88
22	RX J1037.5−5647	unclear	10:37:35.20	−56:47:59.0	10:37:35.302	−56:47:55.82	3.29	11.24
23	1A 1118−615	Be	11:20:57.20	−61:55:00.0	11:20:57.160	−61:55:00.15	0.31	11.59
24	Cen X−3	RLO	11:21:15.10	−60:37:25.5	11:21:15.085	−60:37:25.59	0.14	12.88
25	IGR J11215−5952	Sg	11:21:46.81	−59:51:47.9	11:21:46.813	−59:51:47.93	0.03	9.77
26	2S 1145−619	Be	11:48:00.00	−62:12:25.0	11:48:00.010	−62:12:24.88	0.13	8.65
27	1E 1145.1−6141	Sg	11:47:28.60	−61:57:14.0	11:47:28.546	−61:57:13.39	0.72	12.26
28	4U 1223−624	Sg	12:26:37.60	−62:46:13.0	12:26:37.550	−62:46:13.29	0.46	9.75
29	1H 1249−637	unclear	12:42:50.30	−63:03:31.0	12:42:50.240	−63:03:31.11	0.44	5.14
30	1H 1253−761	unclear	12:39:14.60	−75:22:14.0	12:39:14.460	−75:22:14.26	0.59	6.54
31	1H 1255−567	unclear	12:54:36.90	−57:10:07.0	12:54:36.830	−57:10:07.36	0.69	5.15
32	4U 1258−61	Be	13:01:17.10	−61:36:07.0	13:01:17.090	−61:36:06.64	0.37	12.65
33	4U 1538−52	Sg	15:42:23.30	−52:23:10.0	15:42:23.352	−52:23:9.64	0.59	13.16
34	1H 1555−552	Be	15:54:21.80	−55:19:45.0	15:54:21.760	−55:19:44.36	0.72	8.69
35	IGR J16195−4945	Sg	16:19:32.30	−49:44:30.7	16:19:32.183	−49:44:30.57	0.21	16.37
36	IGR J16465−4507	Sg	16:46:35.26	−45:07:04.5	16:46:35.260	−45:07:04.66	0.16	13.48
37	4U 1700−37	Sg	17:03:56.80	−37:50:39.0	17:03:56.780	−37:50:38.84	0.33	6.42
38	XTE J1739−302	Sg	17:39:11.58	−30:20:37.6	17:39:11.551	−30:20:37.73	0.40	12.64
39	RX J1744.7−2713	Be	17:44:45.70	−27:13:44.0	17:44:45.760	−27:13:44.51	1.00	8.23
40	IGR J17544−2619	Sg	17:54:25.28	−26:19:52.6	17:54:25.270	−26:19:52.59	0.11	11.66
41	RX J1826.2−1450	Be	18:26:15.06	−14:50:54.3	18:26:15.060	−14:50:54.37	0.10	10.80
42	AX 1845.0−0433	Sg	18:45:01.50	−04:33:55.5	18:45:1.589	−04:33:56.73	1.81	12.76
43	3A 1909+048	Sg	19:11:49.60	+04:58:58.0	19:11:49.562	+04:58:57.75	0.63	12.60
44	Cyg X−1	Sg	19:58:21.70	+35:12:06.0	19:58:21.670	+35:12:05.69	0.48	8.54
45	RX J2030.5+4751	Be	20:30:30.80	+47:51:51.0	20:30:30.840	+47:51:50.65	0.54	9.03
46	GRO J2058+42	Be	20:58:47.50	+41:46:37.0	20:58:47.534	+41:46:37.13	0.40	14.13
47	SAX J2103.5+4545	Be	21:03:36.00	+45:45:04.0	21:03:35.700	+45:45:05.52	3.44	13.77
48	1H 2138+579	Be	21:39:30.60	+56:59:12.9	21:39:30.685	+56:59:10.39	2.61	13.82
49	1H 2202+501	unclear	22:01:38.20	+50:10:05.0	22:01:38.210	+50:10:04.63	0.38	9.30
50	4U 2206+543	Be	22:07:56.20	+54:31:06.0	22:07:56.230	+54:31:06.36	0.44	9.74
51	SAX J2239.3+6116	Be	22:39:20.90	+61:16:03.8	22:39:20.839	+61:16:26.59	0.49	14.10
52	HD 259440	Be	06:32:59.26	+05:48:01.2	06:32:59.257	+05:48:01.15	0.01	8.88
53	SAX J0635.2+0533	Be	06:35:18.28	+05:33:06.3	06:35:18.279	+05:33:06.28	0.01	12.50
54	IGR J08262−3736	Be	08:26:13.65	−37:37:11.9	08:26:13.651	−37:37:11.82	0.06	12.16
55	IGR J08408−4503	Sg	08:40:47.79	−45:03:30.2	08:40:47.780	−45:03:30.14	0.15	7.45
56	2FGL J1019.0−5856	Be	10:18:55.59	−58:56:46.0	10:18:55.574	−58:56:45.94	0.11	12.27
57	EXMS B1210−645	Be	12:13:14.79	−64:52:30.5	12:13:14.776	−64:52:30.48	0.10	13.98
58	PSR B1259−63	Be	13:02:47.65	−63:50:08.6	13:02:47.637	−63:50:08.63	0.11	9.63
59	IGR J21347+4737	Be	21:34:20.37	+47:38:00.2	21:34:20.368	+47:38:00.16	0.05	14.00
60	MWC 656	Be	22:42:57.30	+44:43:18.3	22:42:57.298	+44:43:18.21	0.08	8.71
61	SWIFT J0850.8−4219	RSG	08:50:40.08	−42:11:52.3	08:50:40.081	−42:11:51.45	0.92	13.35
62	4U 1954+31	RSG	19:55:42.27	+32:05:48.8	19:55:42.336	+32:05:48.95	0.82	8.36
63	Swift J0243.6+6124	Be	02:43:40.33	+61:26:02.8	02:43:40.424	+61:26:03.76	1.17	12.39

Table 2. Astrometric measurements and radial velocities for the HMXB sample. For each source, we provide parallax, proper motions, and systemic radial velocity.

No.	Source	Spty	Parallax π_t (mas y^{-1})	Proper motion $\mu_\alpha\cos\delta$ (mas y^{-1})	μ_δ (km s^{-1})	Systemic radial velocity V_r	Ref.
1	IGR J00370+6122	B0.5II–III	0.294±0.012	−1.796±0.011	−0.525±0.014	−80.0±3.0	[1]
2	2S 0114+650	B0.5Ib	0.223±0.011	−1.243±0.009	0.761±0.012	−31.0±5.0	[2]
3	4U 0115+634	B0.2Ve	0.174±0.016	−1.684±0.013	0.504±0.017	–	–
4	IGR J01363+6610	B1Ve	0.174±0.011	−1.626±0.009	−0.027±0.011	–	–
5	RX J0146.9+6121	B1Ve	0.367±0.022	−1.029±0.016	−0.082±0.017	−37.0±4.3	[3]
6	IGR J01583+6713	Be	0.167±0.013	−1.198±0.011	0.300±0.013	–	–
7	1E 0236.6+6100	B0Ve	0.405±0.013	−0.423±0.011	−0.256±0.012	−41.41±0.60	[4]
8	V 0332+53	O8.5Ve	0.180±0.020	−0.268±0.020	0.440±0.020	–	–
9	4U 0352+309	B0Ve	1.668±0.037	−1.282±0.053	−1.869±0.030	1.0±0.9	[5]
10	XTE J0421+560	sgB[e]	0.243±0.015	−0.474±0.018	−0.510±0.013	–	–
11	RX J0440.9+4431	B0.2Ve	0.410±0.015	0.101±0.016	−1.186±0.014	–	–
12	EXO 051910+3737.7	B0IVpe	0.759±0.030	1.305±0.041	−3.999±0.028	–	–
13	1A 0535+262	O9.7IIIe	0.560±0.023	−0.590±0.031	−2.880±0.016	−30.0±4.0	[6]
14	1H 0556+286	B5ne	0.626±0.030	0.634±0.034	−2.189±0.021	34	[7]
15	IGR J06074+2205	Be	0.166±0.018	0.573±0.020	−0.608±0.014	–	–
16	XTE J0658–073	O9.7Ve	0.174±0.015	−0.638±0.015	1.256±0.014	–	–
17	3A 0726–260	O8–9Ve	0.130±0.017	−0.881±0.012	1.785±0.018	–	–
18	1H 0739–529	B7IV–Ve	1.544±0.021	−4.572±0.027	8.530±0.028	–	–
19	RX J0812.4–3114	B0.2IVe	0.149±0.012	−1.455±0.011	2.146±0.016	–	–
20	4U 0900–40	B0.5Ib	0.510±0.015	−4.822±0.015	9.282±0.016	−3.2±0.9	[10]
21	GRO J1008–57	B0e	0.282±0.013	−4.702±0.015	3.559±0.014	–	–
22	RX J1037.5–5647	B0V–IIIe	0.197±0.016	−6.305±0.021	3.010±0.018	–	–
23	1A 1118–615	O9.5Ve	0.343±0.011	−5.421±0.012	1.370±0.012	–	–
24	Cen X–3	O6.5II–II	0.145±0.014	−3.121±0.015	2.331±0.014	39±3	[11]
25	IGR J11215–5952	B1Ia	0.138±0.012	−5.147±0.012	2.727±0.013	–	–
26	2S 1145–619	B0.2IIIe	0.489±0.017	−6.226±0.017	1.598±0.018	–	–
27	1E 1145.1–6141	B2Iae	0.121±0.010	−6.226±0.010	2.362±0.012	−13.0±3.0	[12]
28	4U 1223–624	B1–1.5Ia	0.278±0.016	−5.227±0.016	2.071±0.019	4.1±2.4	[13]
29	1H 1249–637	B0.5IIIe	2.299±0.077	−12.857±0.070	−3.677±0.074	22±7	[14]
30	1H 1253–761	B7Vne	4.787±0.027	−27.340±0.034	−8.934±0.040	−20.0±7.4	[14]
31	1H 1255–567	B5Ve	8.294±0.117	−28.386±0.088	−10.447±0.112	13.0±3.7	[14]
32	4U 1258–61	B0.7Ve	0.542±0.014	−4.341±0.012	−0.236±0.015	–	–
33	4U 1538–52	B0Iab	0.176±0.015	−6.711±0.015	−4.111±0.014	−158.0±11.0	[15]
34	1H 1555–552	B2IIIn	0.756±0.018	−3.124±0.020	−3.223±0.016	–	–
35	IGR J16195–4945	B1–2Ia	0.391±0.051	−0.184±0.062	−0.545±0.044	–	–
36	IGR J16465–4507	B0.5I	0.348±0.017	−1.759±0.022	−3.064±0.016	–	–
37	4U 1700–37	O6.5Iaf+	0.668±0.026	2.414±0.028	5.022±0.021	−60	[16]
38	XTE J1739–302	O8Iab(f)	0.534±0.048	−0.427±0.049	3.760±0.033	–	–
39	RX J1744.7–2713	B0.5V–IIIe	0.822±0.024	−0.857±0.024	−2.296±0.016	–	–
40	IGR J17544–2619	O9Ib	0.419±0.027	−0.506±0.029	−0.668±0.018	−46.8±4.0	[17]
41	RX J1826.2–1450	ON6.5V((f))	0.527±0.015	7.425±0.014	−8.151±0.012	17.3±0.5	[18]
42	AX 1845.0–0433	O9.5I	0.184±0.024	−1.366±0.024	−5.595±0.022	–	–
43	3A 1909+048	pec(BeBH)	0.135±0.023	−3.027±0.024	−4.777±0.024	27±13	[11]
44	Cyg X–1	O9.7Iab(BeBH)	0.468±0.015	−3.812±0.015	−6.310±0.017	−2.7±0.9,−7.0±0.5,−5.1±0.5	[19], [20], [21]
45	RX J2030.5+4751	B0.5V–IIIe	0.437±0.016	−2.714±0.020	−4.536±0.018	–	–
46	GRO J2058+42	O9.5–B0IV–Ve	0.109±0.013	−2.21±0.015	−3.351±0.017	–	–
47	SAX J2103.5+4545	B0Ve	0.161±0.013	−3.505±0.014	−3.160±0.013	–	–
48	1H 2138+579	B1–B2Ve	0.133±0.013	−2.964±0.014	−2.204±0.014	–	–
49	1H 2202+501	Be	0.896±0.013	2.365±0.015	−0.294±0.013	−16.8± 2.5	[22]
50	4U 2206+543	O9.5Ve	0.320±0.014	−4.173±0.015	−3.317±0.014	−62.7,−54.5±1.0	[23], [24]
51	SAX J2239.3+6116	B0V–B2IIIe	0.136±0.014	−2.344±0.015	−1.015±0.014	–	–
52	HD 259440	B0pe	0.571±0.023	−0.026±0.020	−0.428±0.016	36.9±.8	[25]
53	SAX J0635.2+0533	B2V–B1IIIe	0.159±0.015	−0.419±0.013	0.405 ±0.013	–	–
54	IGR J08262–3736	OBV	0.194±0.010	−2.367±0.009	3.177 ±0.013	–	–
55	IGR J08408–4503	O8.5Ib–II(f)p	0.455±0.017	−7.465±0.020	6.100 ±0.019	15.3±0.5	[26]
56	2FGL J1019.0–5856	O6V	0.232±0.010	−6.454±0.013	2.256±0.013	33.0±3.0	[27]
57	EXMS B1210–645	B2V	0.301±0.018	−5.953±0.016	0.450±0.021	−42±11*	[28]
58	PSR B1259–63	O9.5Ve	0.461±0.013	−7.093±0.012	−0.342±0.014	0.0±1.0	[29]
59	IGR J21347+4737	B3V	0.112±0.014	−2.212±0.015	−2.558±0.015	–	–
60	MWC 656	B3IVne+sh	0.509±0.018	−3.478±0.016	−3.159±0.017	−14.1±2.1	[30]
61	SWIFT J0850.8–4219	K3–5I	0.132±0.014	−3.533±0.015	4.217±0.016	–	–
62	4U 1954+31	M4I	0.302±0.024	−2.158±0.021	−6.071±0.026	–	–
63	Swift J0243.6+6124	O9.5Ve	0.192±0.011	−0.729±0.010	0.134±0.012	–	–

Spty: spectral type, π_t: zeropoint-corrected parallax., *: Value Case 2

References: [1] Grunhut et al. (2014); [2] Koenigsberger et al. (2003); [3] Sarty et al. (2009); [4] Aragona et al. (2009); [5] Grundstrom et al. (2007); [6] Hutchings (1984); [7] Wilson (1953); [8] Stickland & Lloyd (1994); [9] Thackeray (1970); [10] Stickland et al. (1997); [11] Duflot et al. (1995); [12] Hutchings et al. (1987); [13] Kaper et al. (2006); [14] Kharchenko et al. (2007); [15] Abubekerov et al. (2004); [16] Gies & Bolton (1986); [17] Nikolaeva et al. (2013); [18] Casares et al. (2011); [19] Gies & Bolton (1982); [20] Gies et al. (2003); [21] Gies et al. (2008); [22] Chojnowski et al. (2017); [23] Abt & Bautz (1963); [24] Stoyanov et al. (2014); [25] Moritani et al. (2018a); [26] Gamen et al. (2015a); [27] Strader et al. (2015a); [28] Monageng et al. (2024); [29] Johnston et al. (1994); [30] Casares et al. (2014)

Table 3. Inferred sample distances and peculiar velocities, together with other source properties from the literature.

No.	Source	Pulse Period (s)	Ref.	Orbital Period (day)	Ref.	$V_{\rm pec}$ ($\rm km\,s^{-1}$)	r_{Gaia} (kpc)	$r_{\rm lit}$ (kpc)	Ref.	M_1 ($\rm M_\odot$)	Ref.	M_2 ($\rm M_\odot$)	Ref.
1	IGR J00370+6122	346±6	[1]	15.665±0.006	[2]	$33.0^{+3.4}_{-3.4}$	3.40±0.14	3.3	[3]	$1.4^\dagger$	–	$10.0^{+5.0}_{-5.0}$	[4]
2	2S 0114+650	9475±25	[5]	11.6	[6]	$36.2^{+5.1}_{-4.2}$	4.48±0.23	7.0±3.6	[7]	$1.4^\dagger$	–	$16.0^{+2.0}_{-2.0}$	[8]
3	4U 0115+634	3.61	[9]	24.309±0.021	[9]	$19.7^{+1.8}_{-1.6}*$	5.74±0.54	7–8	[10]	–	–	–	–
4	IGR J01363+6610	–	–	159±2	[11]	$6.9^{+1.8}_{-1.6}*$	5.75±0.36	2	[3]	–	–	–	–
5	RX J0146.9+6121	1404.2±1.2	[12]	330	[13]	$9.2^{+2.1}_{-1.4}$	2.73±0.16	2.2, 2.5±0.6	[14], [15]	$1.4^\dagger$	–	$11.0^{+2.0}_{-2.0}$	[16]
6	IGR J01583+6713	469.2	[17]	3–12	[18]	$7.3^{+2.1}_{-1.7}*$	5.99±0.47	3.4±0.8, 4.0±0.4, 6.4	[15], [17], [19]	–	–	–	–
7	1E 0236.6+6100	–	–	26.4960±0.0028	[20]	$11.0^{+0.8}_{-0.9}$	2.47±0.08	2.0, 2.0±0.2	[21], [22]	$1.4^\dagger$	–	$12.5^{+2.5}_{-2.5}$	[23]
8	V 0332+53	4.4	[24]	34.25±0.10	[24]	$19.3^{+1.8}_{-1.6}*$	5.57±0.63	7	[25]	–	–	–	–
9	4U 0352+309	835	[26]	250±0.6	[27]	$12.2^{+0.9}_{-0.7}$	0.60±0.01	1.30±0.40, 0.7±0.3	[28], [29]	$1.4^\dagger$	–	$14.0^{+3.0}_{-3.0}$	[30]
10	XTE J0421+560	–	–	19.41±0.02	[31]	$12.3^{+1.9}_{-1.7}*$	4.11±0.25	>5	[32]	–	–	–	–
11	RX J0440.9+4431	202.5±0.5	[33]	150±0.2	[34]	$3.4^{+1.5}_{-1.6}*$	2.44±0.09	3.3±0.50	[35]	–	–	–	–
12	EXO 051910+3737.7	–	–	–	–	$16.7^{+1.7}_{-1.6}*$	1.32±0.05	1.7±0.1	[36]	–	–	–	–
13	1A 0535+262	104	[37]	111±0.4	[24], [37]	$41.7^{+4.2}_{-3.8}$	1.79±0.07	2.00±0.70, 2.9	[21], [38]	$1.6^{+0.6}_{-0.6}$	[39]	$7.5^{+2.5}_{-2.5}$	[39]
14	1H 0556+286	–	–	–	–	$25.8^{+1.0}_{-0.8}$	1.60±0.08	0.83	[40]	–	–	–	–
15	IGR J06074+2205	373.2	[41]	–	–	$25.5^{+3.0}_{-2.6}*$	6.03±0.66	4.4±1.0	[42]	–	–	–	–
16	XTE J0658–073	160.4±0.4	[43]	101.20	[43]	$12.4^{+2.3}_{-1.8}*$	5.74±0.50	3.9±0.1	[43]	–	–	–	–
17	3A 0726–260	103.2	[44]	34.5	[44]	$15.3^{+5.6}_{-3.0}*$	7.67±1.00	4.6±1.3, 6.1±0.3	[45], [46]	–	–	–	–
18	1H 0739–529	–	–	–	–	$8.2^{+1.5}_{-1.5}*$	0.65±0.01	0.52	[47]	–	–	–	–
19	RX J0812.4–3114	31.8851	[48]	81.3	[49]	$28.5^{+3.0}_{-3.2}*$	6.70±0.55	11.4, 8.8±4.0	[50], [51]	–	–	–	–
20	4U 0900–40	283	[26]	8.97	[52]	$58.0^{+2.2}_{-1.8}$	1.96±0.06	1.90±0.20	[53]	$2.1^{+0.2}_{-0.2}$	[54]	$26.0^{+1.0}_{-1.0}$	[54]
21	GRO J1008–57	93.587±0.005	[55]	247.5	[56]	$19.9^{+2.0}_{-1.8}*$	3.54±0.17	5	[57]	–	–	–	–
22	RX J1037.5–5647	860±2	[33]	61.0±0.2	[58]	$21.7^{+5.9}_{-4.1}*$	5.06±0.42	5	[50]	–	–	–	–
23	1A 1118–615	405	[26]	24	[59]	$21.5^{+2.3}_{-1.9}*$	2.92±0.10	5±2	[60]	–	–	–	–
24	Cen X–3	4.84	[26]	2.09	[61]	$96.5^{+3.5}_{-3.5}$	6.89±0.65	10±1	[62]	$1.6^{+0.1}_{-0.1}$	[54]	$24.0^{+1.0}_{-1.0}$	[54]
25	IGR J11215–5952	186.78±0.3	[63]	165	[64]	$49.1^{+2.6}_{-2.1}*$	7.27±0.65	8, 6.2	[65], [66]	–	–	–	–
26	2S 1145–619	292.4	[26]	187.5	[26]	$11.5^{+1.5}_{-1.5}*$	2.05±0.07	3.1, 1.4	[67], [68]	$1.4^\dagger$	–	$13.0^{+2.0}_{-2.0}$	[69]
27	1E 1145.1–6141	298±4	[70]	14.37±0.02	[71]	$55.3^{+14.0}_{-8.2}$	8.29±0.70	8	[72]	$1.7^{+0.3}_{-0.3}$	[73]	$14.0^{+4.0}_{-4.0}$	[73]
28	4U 1223–624	696	[74]	41.498±0.002	[75]	$54.3^{+3.6}_{-3.5}$	3.60±0.21	5.3, 1.8±0.4, 4.1	[76], [77], [78]	$1.9^{+0.6}_{-0.6}$	[75]	$43.0^{+10.0}_{-10.0}$	[75]
29	1H 1249–637	14200	[79]	–	–	$23.8^{+7.1}_{-7.3}$	0.44±0.01	$0.30^{+0.04}_{-0.06}$	[47]	$1.4^\dagger$	–	9.6	[80]
30	1H 1253–761	–	–	–	–	$28.2^{+7.7}_{-6.5}$	0.21±1e-3	$0.236^{+0.029}_{-0.039}$	[47]	$1.4^\dagger$	–	$7.5^\dagger$	[81]
31	1H 1255–567	–	–	–	–	$10.8^{+4.1}_{-3.6}$	0.12±2e-3	$0.11^{+0.007}_{-0.008}$	[47]	–	–	–	–
32	4U 1258–61	272	[82]	133	[26]	$24.8^{+1.5}_{-1.6}*$	1.85±0.05	2.4±0.5	[83]	–	–	–	–
33	4U 1538–52	529	[84], [85]	3.73	[84], [85]	$91.7^{+10.8}_{-10.3}$	5.69±0.50	6.4±1.0, 4.5	[86], [87]	$1.0^{+0.2}_{-0.2}$	[54]	$16.0^{+2.0}_{-2.0}$	[54]
34	1H 1555–552	–	–	–	–	$6.3^{+1.5}_{-1.5}*$	1.32±0.03	0.96	[88]	$1.4^\dagger$	–	$19.4^{+5.0}_{-5.0}$	[89]
35	IGR J16195–4945	–	–	3.945±0.005	[90]	$41.1^{+5.2}_{-2.5}*$	2.56±0.33	7	[91]	–	–	–	–
36	IGR J16465–4507	228±6	[92]	30.32±0.02	[93]	$21.0^{+1.7}_{-1.6}*$	2.88±0.14	12.50, $9.50^{+14.1}_{-5.7}$	[93], [94]	–	–	–	–
37	4U 1700–37	67.4?	[95]	3.41	[96]	$72.7^{+6.4}_{-5.8}$	1.50±0.06	1.90±0.30	[97]	$2.0^{+0.2}_{-0.2}$	[54]	$46.0^{+5.0}_{-5.0}$	[54]
38	XTE J1739–302	–	–	51.47±0.02	[98]	$62.5^{+4.1}_{-2.7}*$	1.87±0.17	2.3	[99]	–	–	–	–
39	RX J1744.7–2713	–	–	–	–	$6.6^{+1.6}_{-1.5}*$	1.22±0.04	0.80	[50]	–	–	–	–
40	IGR J17544–2619	11.58±0.03	[100]	12.172±0.007	[101]	$45.1^{+3.9}_{-4.2}$	2.39±0.15	8, 2-4	[102], [103]	$1.4^\dagger$	–	$23.0^{+2.0}_{-2.0}$	[104]
41	RX J1826.2–1450	–	–	3.91	[105]	$90.3^{+3.0}_{-2.9}$	1.90±0.05	2.5±0.1	[105]	$3.7^{+1.3}_{-1.0}$	[105]	$22.9^{+3.4}_{-2.9}$	[105]
42	AX 1845.0–0433	–	–	5.72	[106]	$54.5^{+8.0}_{-2.5}*$	5.44±0.70	3.6, 6.4±0.76	[107], [108]	–	–	–	–
43	3A 1909+048	–	–	13.1	[109]	$57.0^{+10.2}_{-9.4}$	7.42±1.28	5.5±0.2	[110]	$4.3^{+0.4}_{-0.4}$	[111]	$11.3^{+0.6}_{-0.6}$	[111]
44	Cyg X–1	–	–	5.60	[112]	$20.8^{+1.4}_{-1.4}$	2.14±0.07	1.86±0.12	[113]	$21.2^{+2.2}_{-2.2}$	[114]	$40.6^{+7.7}_{-7.1}$	[114]

Table 3 – *continued*

No.	Source	Pulse Period (s)	Ref.	Orbital Period (day)	Ref.	$V_{\rm pec}$ ($\rm km\,s^{-1}$)	r_{Gaia} (kpc)	$r_{\rm lit}$ (kpc)	Ref.	M_1 ($\rm M_\odot$)	Ref.	M_2 ($\rm M_\odot$)	Ref.
45	RX J2030.5+4751	–	–	–	–	$1.7^{+1.5}_{-1.5}$*	2.29±0.08	2.20	[50]	–	–	–	–
46	GRO J2058+42	198	[115]	55.03	[115]	$19.9^{+9.8}_{-3.0}$*	9.18±1.28	9±1	[3]	1.4†	–	18.0†	[80]
47	SAX J2103.5+4545	358.62	[116]	12.68±0.25	[116]	$30.2^{+2.2}_{-1.7}$*	6.20±0.50	6.50±0.90	[117]	–	–	–	–
48	1H 2138+579	66.2	[26], [118]	20.85	[119]	$20.3^{+4.2}_{-2.4}$*	7.50±0.71	3.8±0.6	[120]	–	–	–	–
49	1H 2202+501	–	–	–	–	$30.3^{+1.3}_{-1.1}$	1.12±0.02	0.70	[47]	–	–	–	–
50	4U 2206+543	5554±9	[121]	19.25±0.8	[122]	$24.1^{+1.8}_{-1.6}$	3.12±0.13	2.6	[123]	1.4†	–	$23.5^{+14.5}_{-8.0}$	[124]
51	SAX J2239.3+6116	1247	[125]	262	[126]	$21.6^{+2.9}_{-2.3}$*	7.36±0.76	4.4	[126]	–	–	–	–
52	HD 259440	–	–	308.0±26.0	[127]	$9.4^{+1.3}_{-1.0}$	1.75±0.07	11–17	[128]	1.4	[128]	$15.7^{+2.5}_{-2.5}$	[128]
53	SAX J0635.2+0533	0.034	[129]	11.2±0.5	[130]	$10.5^{+1.6}_{-1.5}$*	6.29±0.59	2.5–5	[131]	–	–	–	–
54	IGR J08262–3736	–	–	–	–	$11.8^{+2.4}_{-2.1}$*	5.15±0.26	6.1	[132]	–	–	–	–
55	IGR J08408–4503	–	–	9.54	[133]	$41.0^{+2.2}_{-2.2}$	2.20±0.08	2.7	[134]	1.4†	–	33.0†	[135]
56	2FGL J1019.0–5856	–	–	16.54	[136]	$35.2^{+2.0}_{-2.2}$	4.31±0.19	$6.4^{+1.7}_{-0.7}$	[137]	1.4†	[138]	$23.0^{+3.0}_{-3.0}$	[138]
57	EXMS B1210–645	–	–	6.7	[139]	$27.4^{+9.5}_{-11.0}$	3.33±0.20	2.8	[140]	–	–	–	–
58	PSR B1259–63	0.0478	[141]	1236.72	[142]	$24.1^{+1.3}_{-1.4}$	2.17±0.06	$2.6^{+0.4}_{-0.3}$	[142]	1.4†	–	$22.5^{+7.5}_{-7.5}$	[142]
59	IGR J21347+4737	–	–	–	–	$18.1^{+9.8}_{-3.9}$*	8.93±1.13	5.8	[140]	–	–	–	–
60	MWC 656	–	–	60.37±0.04	[143]	$10.8^{+2.1}_{-2.0}$	1.97±0.07	2.6±1.0	[144]	$4.1^{+1.4}_{-1.4}$	[144]	$7.8^{+2.0}_{-2.0}$	[143]
61	SWIFT J0850.8–4219	–	–	–	–	$68.8^{+18.9}_{-10.0}$*	7.57±0.80	12	[145]	–	–	–	–
62	4U 1954+31	19400	[146]	1296.64	[146]	$19.7^{+2.2}_{-2.1}$	3.31±0.27	$3.4^{+0.3}_{-0.2}$	[147]	1.4†	–	$9.0^{+4.0}_{-4.0}$	[146]
63	Swift J0243.6+6124	9.86	[148], [149], [150]	28.3±0.2	[151]	$10.4^{+1.6}_{-1.5}$*	5.20±0.31	4.5±0.5	[152]	–	–	–	–

*: $V_{\rm pec,3D}^{\rm iso}$, †: values for which no constraints are available in the literature.

References: [1] in't Zand et al. (2007); [2] den Hartog et al. (2004); [3] Reig et al. (2005a); [4] González-Galán et al. (2014); [5] Wang (2011); [6] Crampton et al. (1985); [7] Reig et al. (1996); [8] Hu et al. (2017); [9] Rappaport et al. (1978); [10] Negueruela & Okazaki (2001); [11] Corbet & Krimm (2010); [12] Haberl et al. (1998); [13] Sarty et al. (2009); [14] Coe et al. (1993); [15] Reig et al. (2016); [16] Reig et al. (1997); [17] Kaur et al. (2008); [18] Wang (2010); [19] Masetti et al. (2006b); [20] Gregory (2002); [21] Steele et al. (1998); [22] Frail & Hjellming (1991); [23] Casares et al. (2005a); [24] Stella et al. (1985); [25] Negueruela et al. (1999); [26] Nagase (1989); [27] Delgado-Martí et al. (2001); [28] Fabregat et al. (1992); [29] Lyubimkov et al. (1997); [30] Grundstrom et al. (2007); [31] Barsukova et al. (2005); [32] Robinson et al. (2002); [33] Reig & Roche (1999b); [34] Ferrigno et al. (2013); [35] Reig et al. (2005b); [36] Polcaro et al. (1989); [37] Priedhorsky & Terrell (1983b); [38] Lyuty & Zaĭtseva (2000); [39] Hutchings (1984); [40] Bonnet-Bidaud & van der Klis (1981); [41] Reig & Zezas (2018); [42] Reig et al. (2010); [43] McBride et al. (2006); [44] Corbet & Peele (1997); [45] Corbet & Mason (1984); [46] Negueruela et al. (1996); [47] Chevalier & Ilovaisky (1998); [48] Reig & Roche (1999a); [49] Corbet & Peele (2000); [50] Motch et al. (1997); [51] Reig et al. (2001); [52] van der Klis & Bonnet-Bidaud (1984); [53] Sadakane & Hirata (1985); [54] Falanga et al. (2015); [55] Stollberg et al. (1993); [56] Okazaki & Negueruela (2001); [57] Coe et al. (1994); [58] Cusumano et al. (2013); [59] Staubert et al. (2011); [60] Janot-Pacheco et al. (1981); [61] Kelley et al. (1983); [62] Hutchings et al. (1979); [63] Swank et al. (2007); [64] Sidoli et al. (2007); [65] Negueruela et al. (2005); [66] Sidoli et al. (2006); [67] Negueruela (1998); [68] Hutchings et al. (1981); [69] Stevens et al. (1997); [70] Lamb et al. (1980); [71] Ray & Chakrabarty (2002); [72] Ilovaisky et al. (1982); [73] Hutchings et al. (1987); [74] Sato et al. (1986); [75] Kaper et al. (2006); [76] Kaper et al. (1995); [77] Parkes et al. (1980b); [78] Leahy (2002); [79] Torrejón & Orr (2001); [80] Zorec et al. (2005); [81] Waters et al. (1989); [82] Priedhorsky & Terrell (1983a); [83] Parkes et al. (1980a); [84] Becker et al. (1977); [85] Davison et al. (1977); [86] Reynolds et al. (1992); [87] Clark (2004); [88] Grillo et al. (1992); [89] Fairlamb et al. (2015); [90] Cusumano et al. (2016); [91] Sidoli et al. (2005); [92] Lutovinov et al. (2005); [93] Clark et al. (2010); [94] Smith (2004); [95] Murakami et al. (1984); [96] Jones et al. (1973); [97] Ankay et al. (2001); [98] Drave et al. (2010); [99] Negueruela et al. (2006); [100] Romano et al. (2015); [101] Nikolaeva et al. (2013); [102] González-Riestra et al. (2004); [103] Pellizza et al. (2006); [104] Bikmaev et al. (2017); [105] Casares et al. (2005b); [106] Goossens et al. (2013); [107] Coe et al. (1996); [108] Coleiro & Chaty (2013); [109] Crampton & Hutchings (1981); [110] Blundell & Bowler (2004); [111] Picchi et al. (2020); [112] LaSala et al. (1998); [113] Reid et al. (2011); [114] Miller-Jones et al. (2021); [115] Wilson et al. (1998); [116] Baykal et al. (2000); [117] Reig et al. (2004); [118] Koyama et al. (1991); [119] McBride et al. (2007); [120] Bonnet-Bidaud & Mouchet (1998); [121] Finger et al. (2010); [122] Corbet et al. (2007); [123] Blay et al. (2006); [124] Hambaryan et al. (2022); [125] in't Zand et al. (2001); [126] in't Zand et al. (2000); [127] Moritani et al. (2018b); [128] Aragona et al. (2010); [129] Cusumano et al. (2000); [130] Kaaret et al. (2000); [131] Mereghetti & La Palombara (2009); [132] Masetti et al. (2012); [133] Gamen et al. (2015b); [134] Leyder et al. (2007); [135] Gamen et al. (2015a); [136] An et al. (2015); [137] Marcote et al. (2018); [138] Strader et al. (2015b); [139] Walter et al. (2015); [140] Masetti et al. (2009); [141] Manchester et al. (1995); [142] Miller-Jones et al. (2018); [143] Williams et al. (2010); [144] Casares et al. (2012); [145] De et al. (2024); [146] Hinkle et al. (2020); [147] Fortin et al. (2023); [148] Kennea et al. (2017); [149] Jenke & Wilson-Hodge (2017); [150] Bahramian et al. (2017); [151] Doroshenko et al. (2018); [152] Reig et al. (2020)

4 KINEMATICS

All HMBs in our sample have five-parameter astrometric solutions in DR3, viz. celestial positions (right ascension α and declination δ), proper motions ($\mu_\alpha \cos \delta$, hereafter $\mu_{\alpha*}$, and μ_δ) and parallax (π). Note that we use the estimate of the true parallax (π_t) defined in Section 3 for estimating peculiar velocities (V_{pec}).

In order to estimate the 3-D V_{pec} of a source, we need one final measurement — the systemic radial velocity (V_r) of the binary. Although the *Gaia* archive provides radial velocity estimates for some sources, these cannot be used for our study. For close binary systems, such as those in our sample, the systemic radial velocity we require is that of the centre of mass. By contrast, *Gaia* currently provides only an estimate of the radial velocity of the optically luminous component, which will be affected — and usually dominated — by its orbital motion. We have therefore instead compiled V_r estimates from the literature. These are available for 28 of our systems (10 SgXRBs, 12 BeXRBs, 1 RLO, and 5 of unclear classes) as shown in Table 2. When multiple radial velocity measurements were available in the literature, the most recent value based on detailed analysis was preferred, as this usually represented improvements resulting from use of modern instrumentation and revisitation of older observations leading to reduced uncertainties. For the remaining sources without literature V_r values, we first estimate the 2-D V_{pec} ($V_{pec,2D}$) in the plane of the sky by assuming that the radial velocity is entirely associated with Galactic rotation. We then assume that the peculiar velocities are distributed isotropically, which allows us to estimate the 3-D V_{pec} ($V_{pec,3D}$) by applying a correction factor of $4/\pi$. This factor is the ratio of the expectation values of the $V_{pec,3D}$ and $V_{pec,2D}$ values ($\langle V_{pec,3D} \rangle / \langle V_{pec,2D} \rangle$) for an isotropically distributed sample (Hobbs et al. 2005). Additional tests of the isotropic assumption will be described in Section 6.2.

In our calculations, we first calculate velocities in an equatorial Cartesian system, following ESA (1997). We then convert these components to a Galactic Cartesian system. Solar motion and circular Galactic rotation are removed following Reid et al. (2009), yielding the desired V_{pec}, which is relative to our sources' expected motion in the Galactic plane (Gandhi et al. 2020). The Cartesian components of solar motion relative to the local standard of rest ($U_\odot$, $V_\odot$, and $W_\odot$ are 8.0 ± 0.9, 12.4 ± 0.7, and 7.7 ± 0.9 km s^{-1}, respectively) and Galactic rotation speed at Solar distance ($\Theta_0 = 236 \pm 3$ km s^{-1}) from the Galactic centre ($R_0 = 8.2 \pm 0.1$ kpc) are taken from the work of Kawata et al. (2019). We estimate uncertainties via Monte Carlo resampling of all relevant parameters, including the Galactic constants. When quoting uncertainties, we adopt the highest-density interval (HDI)[3] containing 68.27 per cent of the Monte Carlo samples. For systems without available V_r measurements with the isotropic correction of $4/\pi$, an additional uncertainty term of 0.18 dex in log V_{pec} was included. This term was determined from simulations of isotropically distributed velocities and accounts for the scatter introduced when converting from 2D to 3D velocities. (e.g., Blaauw 1961)

It is important to emphasize that the true space velocities of HMXBs can only be accurately determined if the system's birthplace is known (for example, the origin of 4U 1700–37 in NGC 6231; see van der Meij et al. 2021). Without knowledge of the birthplace, velocities are best estimated relative to the Local Standard of Rest (LSR). However, massive stars in the Galactic plane commonly exhibit deviations of about 20 km s^{-1} from the LSR (Carlberg
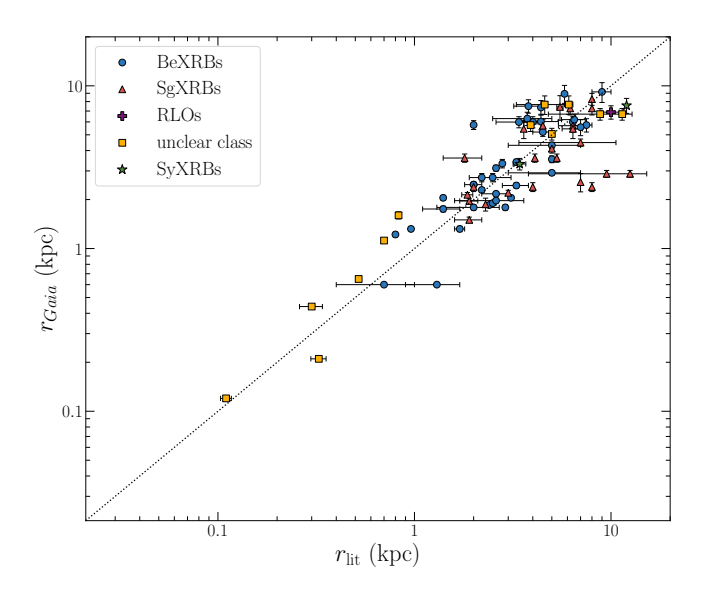

Figure 1. Comparison of *Gaia* DR3 distances (r_{Gaia}) with literature estimates (r_{lit}) for our HMXBs, where known. The dotted line denotes the equality relation $r_{lit} = r_{Gaia}$. Symbols represent different spectral classes. Sources scatter around the equality relation, and there is no obvious bias as a function of spectral class.

---

et al. 1985), implying that the velocities we derive may not precisely represent their true three-dimensional motions.

5 RESULTS

Fig. 1 compares our *Gaia*-based distances (r_{Gaia}) with literature values (r_{lit}), overlaid with a dotted line denoting the 1:1 relation ($r_{Gaia} = r_{lit}$) and using symbols to indicate different spectral classes. The agreement between the parallax-based and literature estimates is generally reasonable, despite some scatter, and there are no obvious systematic dependencies on spectral class. In principle, the *Gaia* geometric parallax estimates should be more reliable than literature distances, which often rely on heterogeneous, model-dependent methods. Some HMXBs in our sample have more than one reported distance, although not all of these have associated uncertainties. Our distance estimates and their uncertainties are listed in Table 3, with notes on individual sources provided later, and we find that the *Gaia* distances derived via parallax inversion agree with the Bayesian estimates reported for HMXBs by Zhao et al. (2023). To further investigate the residual scatter in the figure, we checked the values of their Gaia-reported astrometric excess noise and Re-normalised Unit Weight Error (RUWE). These parameters are indicative of residuals relative to the Gaia pipeline single-star astrometric fits. Values significantly in excess of 0 for the astrometric excess noise, and values in excess of 1.4 for RUWE could indicate a poor single-star fit, which may result from instrumental or pipeline artefacts, or arise from the presence of inherent stellar multiplicity (cf. Belokurov et al. 2020; Gandhi et al. 2022). Our targets are specifically selected to be binaries and, indeed, we did not find any systematic trends with RUWE or astrometric excess noise. This implies that even if single-star fitting accounts for some the scatter between r_{Gaia} and r_{lit}, there is no obvious bias for individual source distances.

Source kinematics were computed using the algorithm described in Section 4. In addition, by generating 50,000 mock samples through Monte Carlo resampling of all parameters, including the adopted Galactic constants, we derived probability distributions of V_{pec} for

---

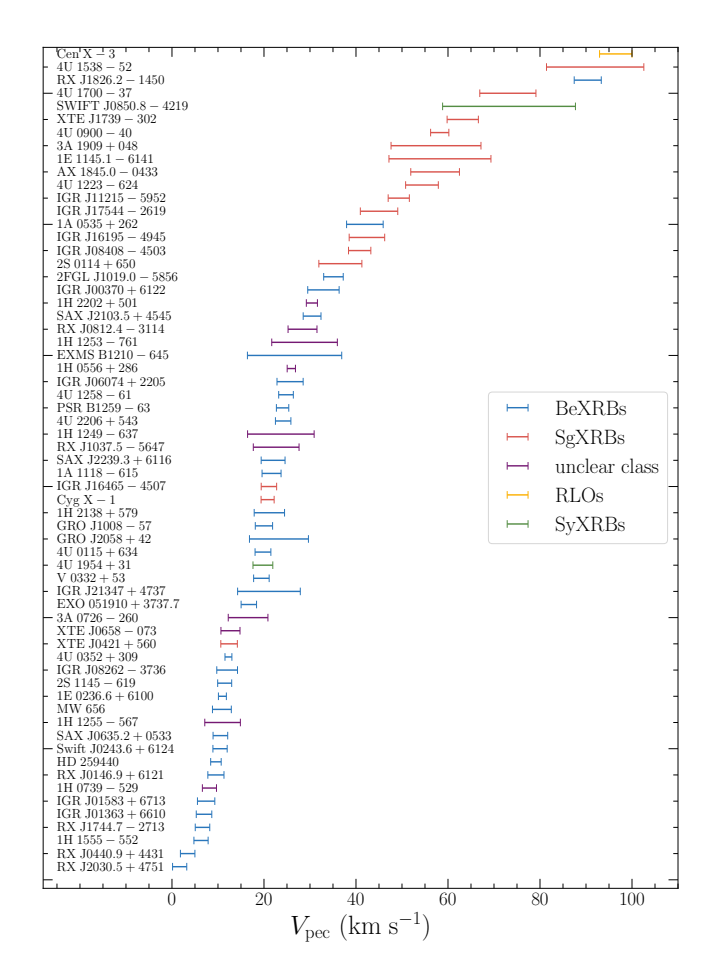[3] https://github.com/aloctavodia/BAP/blob/master/first_edition/code/Chp1/hpd.py

Figure 2. Highest-density (68.27 per cent) intervals of V_{pec} for 63 HMXBs. Source names are annotated on the left. Sources are sorted by V_{pec} in ascending order from the bottom, and are colour-coded by HMXB class.
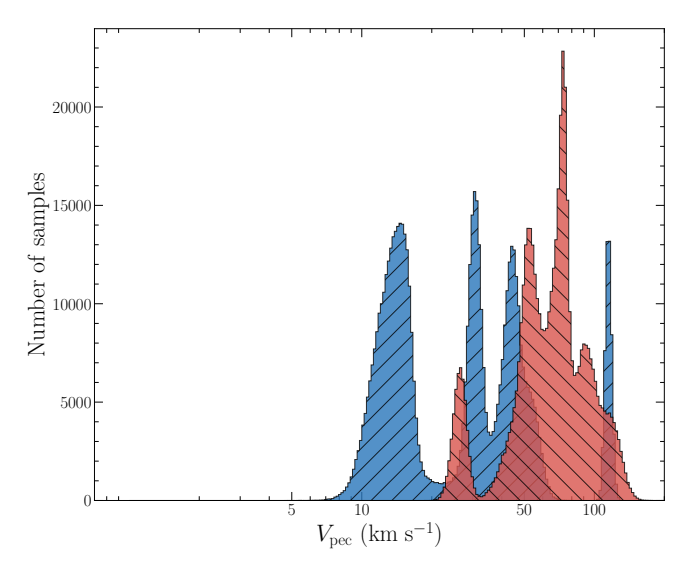

Figure 3. Summed distributions of V_{pec} for BeXRBs (blue, right-angled hatching '/') and SgXRBs (red, left-handed hatching '\'; colours online). Only systems with available V_r values are included here. For each source, 50,000 random samples are drawn. The BeXRBs system with the highest V_{pec} velocity is RX J1826.2–1450/LS 5039 – its distribution stands out from its subgroup on the far right. Similarly, Cyg X–1 is the SgXRB with the smaller V_{pec}, ≈ 20 km s^{-1}, separated from other SgXRBs.
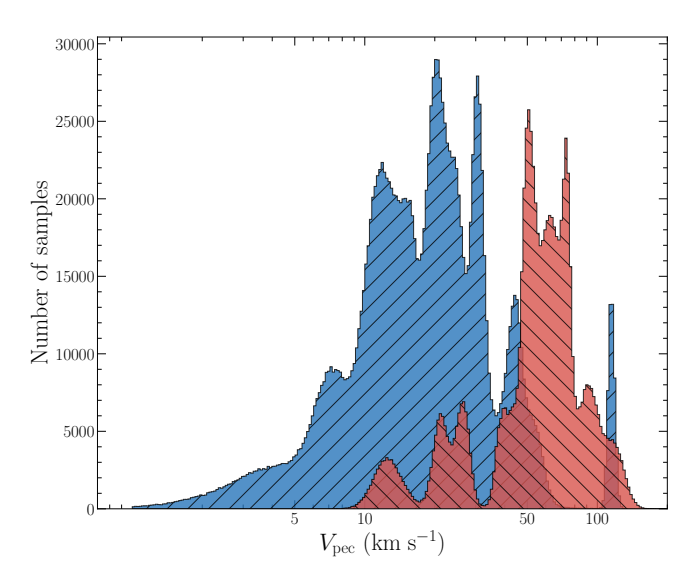
Figure 4. Histogram of V_{pec} values as in Fig. 3, but now also incorporating $V_{pec,3D}^{iso}$ as a proxy for systems without established radial velocities.

all systems. These distributions, categorised by their respective sub-groups, are presented in Appendix Fig. 13 and 14.

Fig. 2 is a summary of these V_{pec} confidence regions for each source. Sources are sorted by their V_{pec} values and colour-coded by HMXB sub-classes. It is easily apparent from the figure that SgXRBs have larger V_{pec} values than BeXRBs. The estimated V_{pec} values of HMXBs are tabulated in Table 3, with a full range spanning ≈ 2—97 km s^{-1} and an average of 29.0 ± 2.8 km s^{-1}, where the uncertainty represents the standard error. The single highest V_{pec} value is associated with the RLO system Cen X–3 ($V_{pec} = 96.5 \pm 3.5$ km s^{-1}). However, this is the only RLO HMXB in our sample. More data will be needed to determine if there is a tendency for RLO systems to be fast movers.

Focusing on the two more sizeable sub-samples, we find that the mean V_{pec} values for BeXRBs and SgXRBs are 20.9±3.5 and 58.0±6.6 km s^{-1}, respectively. This difference persists even with the restricted subset of HMXBs that have measured V_r values. For reference, the velocity dispersion of young stellar populations is approximately 20 km s^{-1} (Carlberg et al. 1985).

We illustrate this difference between these two classes again with the histogram in Fig. 3. Here, 50,000 values for each of these HMXBs were randomly sampled from their respective V_{pec} distributions. These sample distributions are then summed for the BeXRBs and SgXRBs separately. Amongst the BeXRBs, RX J1826.2–1450/LS 5039's distribution appears to be an outlier. Similarly, Cyg X-1 has a

low V_{pec} (≈ 20 km s^{-1}) compared to other SgXRBs. In the Appendix, the reader can find larger figures with individual systems annotated.

In Fig. 4, we show the V_{pec} distribution for all 49 systems with or without measured V_r values. Both Figs. 3 and 4 clearly demonstrate a significant difference in the mean velocities between BeXRBs and SgXRBs. Including or excluding systems without measured radial velocities does not change this inference, pointing to a robust difference between the classes.

To quantitatively assess this difference, we performed a Kolmogorov-Smirnov test (K-S test) using the `ks_2sample` package
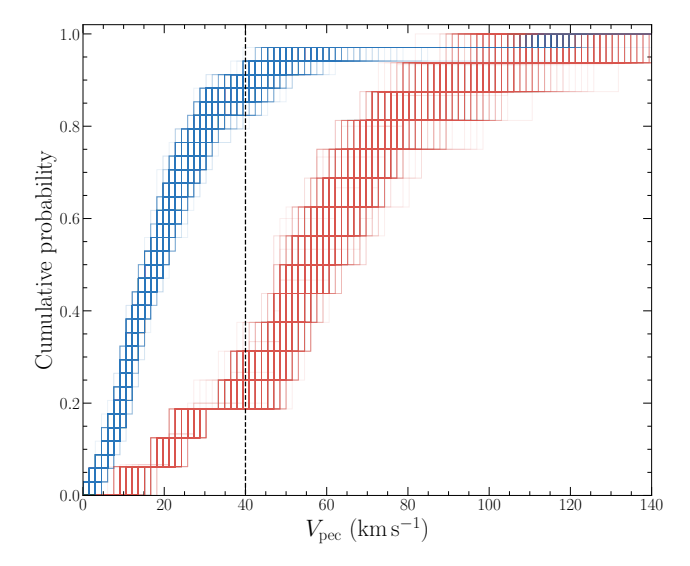
Figure 5. Cumulative distribution of V_{pec} for BeXRBs (blue) and SgXRBs (red). Roughly half of the BeXRBs have V_{pec} lower than 20 km s^{-1}, with nearly all of them being slower than 30 km s^{-1}. In contrast, around half of SgXRBs have $V_{pec} \leq 50$ km s^{-1}. The two subgroups are optimally separated around a threshold of 40 km s^{-1}, represented by the vertical dashed line.

within the SCIPY[4] library (Virtanen et al. 2020). The null hypothesis is that the V_{pec} values for BeXRBs and SgXRBs are drawn from the same underlying distribution. We created 1,000 random ensembles of V_{pec} by drawing one random sample from the V_{pec} distributions of each system. The K-S test is then performed on each of the 1,000 random ensembles, from which we obtained a distribution of test statistics and p-values. We found that 100 per cent of the test results reject the null hypothesis, implying a significant difference between the SgXRBs and BeXRBs V_{pec} distributions.

In Fig. 5, the cumulative distribution shows that around 50 per cent of BeXRBs have V_{pec} below 20 km s^{-1}, and 80 per cent of them are slower than 30 km s^{-1}. On the other hand, half of the SgXRBs sample exhibits V_{pec} values exceeding 50 km s^{-1}. The two sub-groups are maximally separated at a velocity of approximately 40 km s^{-1}. Accordingly, we adopt this value as our velocity separation threshold: systems with V_{pec} equal to or greater than 40 km s^{-1} are classified as having *high* peculiar velocities, while those with V_{pec} less than 40 km s^{-1} are classed as *low* peculiar velocity systems. Although *low* can be relative, a space velocity of less than 40 km s^{-1} is still substantially higher than the typical sound speed in most regions of the Galactic plane. Interestingly, three-quarters of SgXRBs exhibit V_{pec} exceeding this threshold.

There are 33 systems that have available orbital and spin periods, listed in Table 3. To investigate any potential associations between V_{pec} and the spin or orbital periods, we visualise the distribution of these periods in Fig. 6. This shows a Corbet diagram (Corbet 1986) for these systems, with V_{pec} values depicted by symbol size. It is immediately apparent that sources also show some degree of separation in the Corbet parameter space. These V_{pec} values and corresponding implications will be discussed in Section 6.

6 DISCUSSION

The birth of compact objects is expected to leave an imprint on their subsequent kinematics and evolution. These can be constrained in binaries where the companion star traces the orbit of the system. In this work, we have leveraged state-of-the-art astrometry from *Gaia* DR3 to measure the complete (three-dimensional) systemic motions of Galactic HMXBs in excess of Galactic rotation that have been perturbed by natal kicks. Our results presented in Section 5 quantify the moments of the three-dimensional kinematic distributions for the full sample, and reveal differences between HMXB classes; we extend previous studies that were either restricted to two-dimensional velocities or could not clearly reveal such differences (Chevalier & Ilovaisky 1998; Fortin et al. 2022). Recent studies of larger samples including black holes as well as neutron stars in binaries find wider V_{pec} distributions extending to several hundred km s^{-1} (e.g. Zhao et al. 2023); our work here has focused on the more massive of such systems, which tend to have lower peculiar motions, on average, presumably also indicative of weaker corresponding natal kicks. But we also hone in on the various sub-classes of HMXBs to explore their properties in more detail than before.

A global anti-correlation between total mass and V_{pec} across all types of compact object binaries – including HMXBs *and* LMXBs – has previously been identified by Zhao et al. (2023). Since M_{tot} is the primary difference between LMXBs and HMXBs, this trend *across* classes need not necessarily apply *within* classes. In Fig. 7, we therefore show what this parameter space looks like when we focus specifically on HMXBs. Formally, a Spearman rank test yields a marginally significant *positive* correlation for these systems (correlation coefficient = 0.46, p-value = 0.02). To the extent that the correlation is real, Fig. 7 suggests that it is induced by systematic differences in mass and V_{pec} between different HMXB sub-types. Given the unclear statistical significance of this trend, we will not discuss it further in the present study. However, it would clearly be worth revisiting this topic when additional data become available.

We now discuss some of the implications of our results.

6.1 Comparison of kinematics between SgXRBs and BeXRBs

What is the underlying cause of the difference between the sub-types? One possibility can be traced back to differences in the pre-SN progenitors of their compact objects. SgXRBs are thought to inhabit binary systems with tighter orbits, on average, as compared to BeXRBs. They are thus expected to have higher relative orbital velocities between the two binary components at the point of SN. Following the kinematic formulation of Kalogera (1996), we expect the average runaway velocity to be of a similar order to the relative orbital velocity, and thus be larger for SgXRBs.

This scenario was first pointed out by van den Heuvel et al. (2000). Their study proposed that the kinematic differences between Be and Sg system may be tracable to two main factors. The first factor is related to a higher probable fractional helium core mass of the progenitor stars of SgXRBs compared to those of BeXRBs. A higher primary mass for SgXRBs leads to a higher helium core mass and, in turn, a smaller increase in the orbital period during the initial mass transfer from the primary to the companion, resulting in tighter pre-supernova (pre-SN) orbits and higher orbital velocities for the helium core. The second proposed factor is a proportionally smaller mass ejection in Be systems compared to supergiants during the SN event. We will return to these points in Section 6.3.

Fortin et al. (2022) confirm that BeXRBs possess systems with relatively low mass and low peculiar velocities. Furthermore, in one
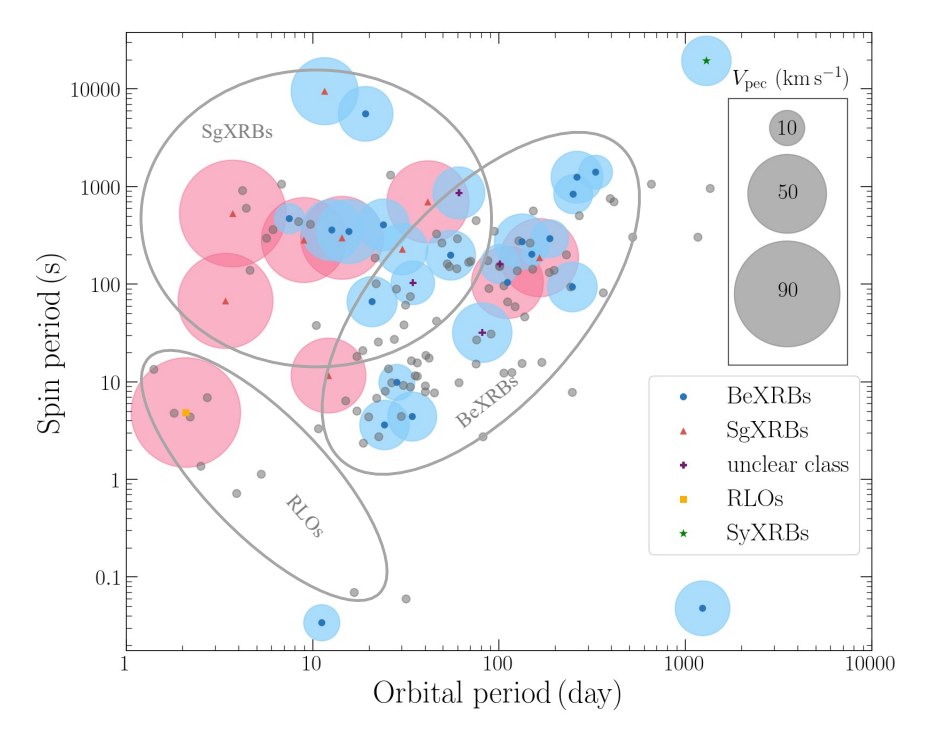
Figure 6. The Corbet diagram (colours online) plotting spin vs. orbital period for HMXBs in this study; different systems are further distinguished by the colour of the crosses: blue, BeXRBs; red, SgXRBs; Magenta, unclear classes; yellow, RLOs. The V_{pec} values are mapped to the sizes of circles around the crosses. Red and blue circles indicate systems with V_{pec} greater and lower than 40 km s^{-1}, respectively. Additionally, filled grey circles mark the loci of other Galactic and extragalactic HMXBs from Small Magellanic Cloud, and Large Magellanic Cloud.
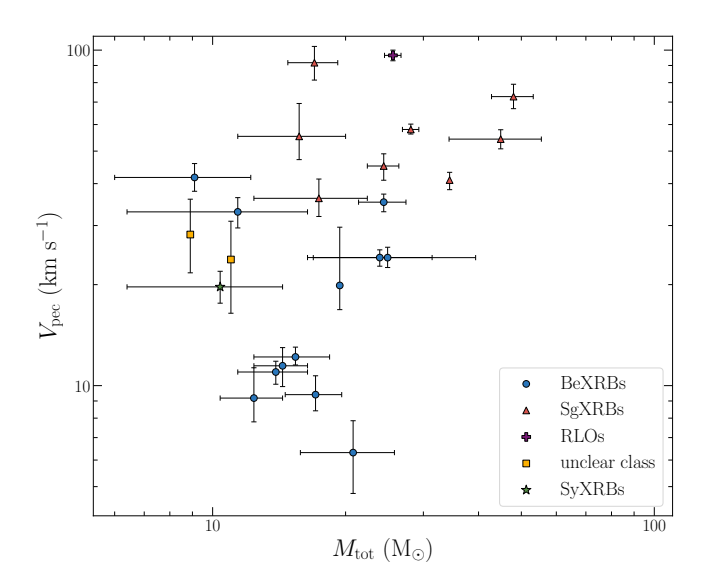
Figure 7. The relationship between total mass (M_{tot}) and V_{pec} for NS HMXBs, including their associated uncertainties. Systems are distinguished by cross colour according to sub-classes: blue for BeXRBs, red for SgXRBs, green for SyXRBs, magenta for unclear classifications, and yellow for RLOs.

BeXRB system at the extreme end of the BeXRBs mass scale, RX J1826.2–1450/LS 5039, hosting an Oe-type donor, the runaway velocity V_{pec} is also extreme, at ≈ 89.1 km s^{-1}. By contrast, the other Oe-type objects studied display V_{pec} values between 20 and 40 km s^{-1}. On the other hand, the SgXRBs display a consistently high peculiar velocity, with little to no relationship to mass (Fortin et al. 2022).

For systems in which the accretor is a neutron star, it is interesting to check whether/how the peculiar velocity of systems relates to their position in the so-called Corbet diagram, i.e. to their orbital and spin periods (P_{orb} and P_{spin}, respectively). Fig. 6 shows this diagram with both sub-classes and peculiar velocities added. This confirms that V_{pec} can provide useful supplementary information for classifying HMXBs. Nonetheless, it should be noted that there are exceptions. That is, position in the Corbet diagram does not *cleanly* correlate with either HMBX sub-class, nor with V_{pec}. Nevertheless, the difference in the characteristic peculiar velocities of BeXRBs and SgXRBs, in particular, is also clearly reflected in the Corbet diagram.

Knigge et al. (2011) showed that BeXRBs appear to fall into two distinct sub-populations: systems with short P_{spin} ($\lesssim 30$ s) and systems with long P_{spin} ($\gtrsim 30$ s). They suggested that the low-P_{spin} group may originate from low-kick electron-capture supernovae, in which case they should exhibit lower space velocities than those with long P_{spin}. We have attempted to test this suggestion. Within our set of BeXRBs, a K-S test reveals no statistically significant difference between these two P_{spin} groups as indicated by the very small p-value. However, there are only five systems in the short spin-period category in our sample, so this test has very limited statistical power. We can therefore not conclusively confirm or reject this possibility.

6.2 Isotropy of Peculiar Motions

Analysis of the full 3-D peculiar motions of sources requires knowledge of V_r. However, V_r values are known only for 28 of our sample systems. For the remaining systems, we have made the assumption of isotropicity. This is the minimal ansatz that applies if there is no special directionality to the motions of HMXBs in the Galactic potential, as seen by us. Here, we conduct a basic test on the viability of this ansatz.

Table 4. The calculated $\langle V_{pec,3D}\rangle/\langle V_{pec,2D}\rangle$ values for each plane and the p-values from the K-S test compared to the theoretical prediction under the assumption of isotropy.

$V_{pec,2D}^a$	$\langle V_{pec,3D}\rangle/\langle V_{pec,2D}\rangle^b$	p-value^c
UV plane	1.20	0.06
UW plane	1.33	0.19
VW plane	1.40	0.45
Theoretical prediction assuming isotropy	$4/\pi$ (1.27)	–

^{a}: The considered plane of $V_{pec,2D}$
^{b}: The ratio between the average $V_{pec,3D}$ and the average $V_{pec,2D}$
^{c}: p-value resulting from the comparison between each plane and 10 million theoretical predictions were obtained using K-S test

Such an ansatz was first introduced for compact object motions in the pioneering study of Hobbs et al. (2005) who utilised the 2-D proper motions of pulsars to infer the properties of 3-D velocity distributions. In a statistical sense, the expected $\langle V_{pec,3D}\rangle/\langle V_{pec,2D}\rangle$ for a Maxwell distribution of velocities is expected to be $4/\pi$. We can test this directly for sources with full 3-D kinematic information.

For the 28 objects with measured V_r, we can compute $V_{pec,2D}$ by treating them as if their radial velocities are unknown. The 3-dimensional $V_{pec,3D}$ represents the resultant vector of space velocity in Cartesian coordinates (U_s[5], V_s[6], and W_s[7]), resulting in three possible cases for $V_{pec,2D}$ (UW, UV, and VW plane). The calculated $\langle V_{pec,3D}\rangle/\langle V_{pec,2D}\rangle$ values in each plane are shown in Table 4. For these three cases, closely aligning with the expected ratio of $4/\pi$, validating the underlying assumption. We compared the ratio between $V_{pec,3D}$ and $V_{pec,2D}$ with the theoretical prediction from a simulation which is drawn from 10 million random samples as shown in Fig. 8. We also tested the differences between the theoretical prediction and our estimated values using the K-S test. For the UW and VW planes, the test results indicate strong consistency between empirical data and simulations. However, for the UV plane, the K–S test yielded a p-value of 0.06—marginally above the conventional significance threshold of 0.05—suggesting only tentative agreement and highlighting the need for further investigation into this particular component.

Fig. 9 shows the Gaia DR3 map displaying the positions of 63 HMXBs projected onto the Galactic plane, taking into account distance uncertainties and the different colours representing 4 subclasses and unclear class. The 28 arrows displayed on the plot represent the $V_{pec,2D}$ vectors on the UV plane, indicating both their length and direction for 28 known V_r sources. Notably, the distribution of the $V_{pec,2D}$ vectors on the UV plane suggests isotropy, indicating a uniform and consistent pattern across the Galactic plane.

Based on the discussion mentioned above, we assume that the $V_{pec,2D}$ would be the smallest magnitude relative to the Galactic rotation. Therefore, $V_{pec,min}$ can be considered as 2-D speeds. In order to estimate 3-D speeds, we use the assumption mentioned above (i.e., isotropy of the velocity vector) multiplied by a constant, referred to as $V_{pec,3D}^{iso}$. The $V_{pec,3D}^{iso}$ values in this study correspond with Fortin et al. (2022). Therefore, we use this estimation to assume $V_{pec,3D}^{iso}$ for systems with no established V_r. Even though, there are ambiguously estimated $V_{pec,3D}^{iso}$ values for systems with no literature V_r, we can still

[5] U_s: Radial component of V_{pec} in the Galactic plane
[6] V_s: Azimuthal component of V_{pec} relative to local Galactic rotation
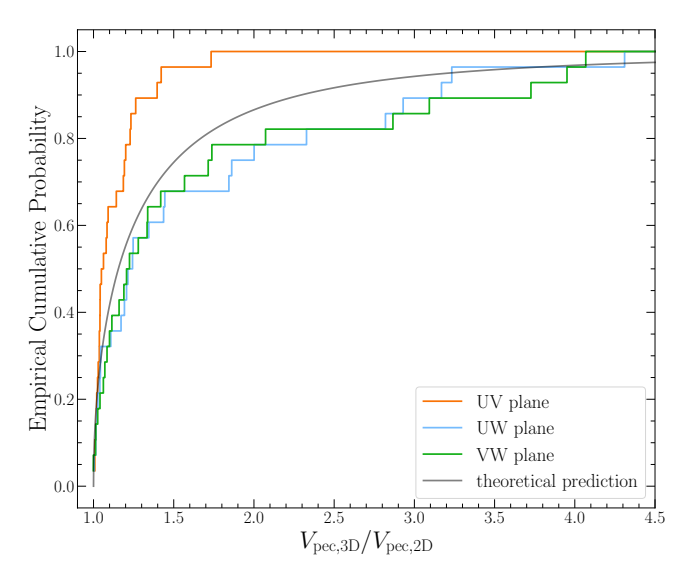[7] W_s: V_{pec} component perpendicular to the Galactic plane

Figure 8. The empirical cumulative distribution of the ratio between 3-D and 2-D of V_{pec}. There are three possible cases for $V_{pec,2D}$ ($V_{pec,2D}$ on UW, UV, and VW plane) and 10 million theoretical predictions. The distribution suggests that when using $V_{pec,2D}$ from the UW and VW planes, the resulting ratios align closely with the theoretical predictions. Furthermore, results from the K-S test, p value, indicate that $V_{pec,2D}$ on the UV plane shows no significant deviation from the theoretical predictions.

see the different velocities between BeXRBs and SgXRBs as shown in Fig. 3.

6.3 Testing the Origin of Class Kinemetic Differences with Binary Population Synthesis

van den Heuvel et al. (2000) suggest that the kinematic differences between the classes could arise from differences in progenitor properties – specifically, the fractional mass-loss of the compact object progenitor through supernova (SN) and the pre-SN system orbital period. Testing this requires estimating the system properties at the time of SN. For this purpose, our team has begun to develop detailed simulations using 'COMPACT OBJECT SYNTHESIS AND MONTE CARLO INVESTIGATION CODE (COSMIC)', a binary population synthesis code derived from the BINARY STELLAR EVOLUTION (BSE) framework, enhanced with updated evolutionary prescriptions and parameters (Breivik et al. 2020). Full details of our efforts will be presented in an upcoming work (Dashwood Brown et al., in preparation). One previous example case study on a black hole XRB – H 1705−250 – outlines the most salient details of our methodology and can be found in Dashwood Brown et al. (2024).

In short, we simulate a large number of binaries, encompassing a broad range of initial parameters for the progenitor zero-age main sequence binary component masses, orbital period, and subsequent evolutionary pathways. In our simulations, stellar winds and mass transfer are treated according to Vink et al. (2001); Vink & de Koter (2005); initial stellar metallicities range $0.1 - 2\,Z_\odot$; and we adopt a delayed SN mechanism, as outlined by Fryer et al. (2012). Mass-loss from the SN progenitor star induces a kick to the centre-of-mass of the system (Nelemans et al. 1999), and additional isotropic natal kicks are included for the resultant compact objects. These simulations are run to find binaries that survive the first SN and form an accreting compact object, searching for systems that end up matching the current observed properties of known XRBs. We match the current observed parameters (component masses, orbital
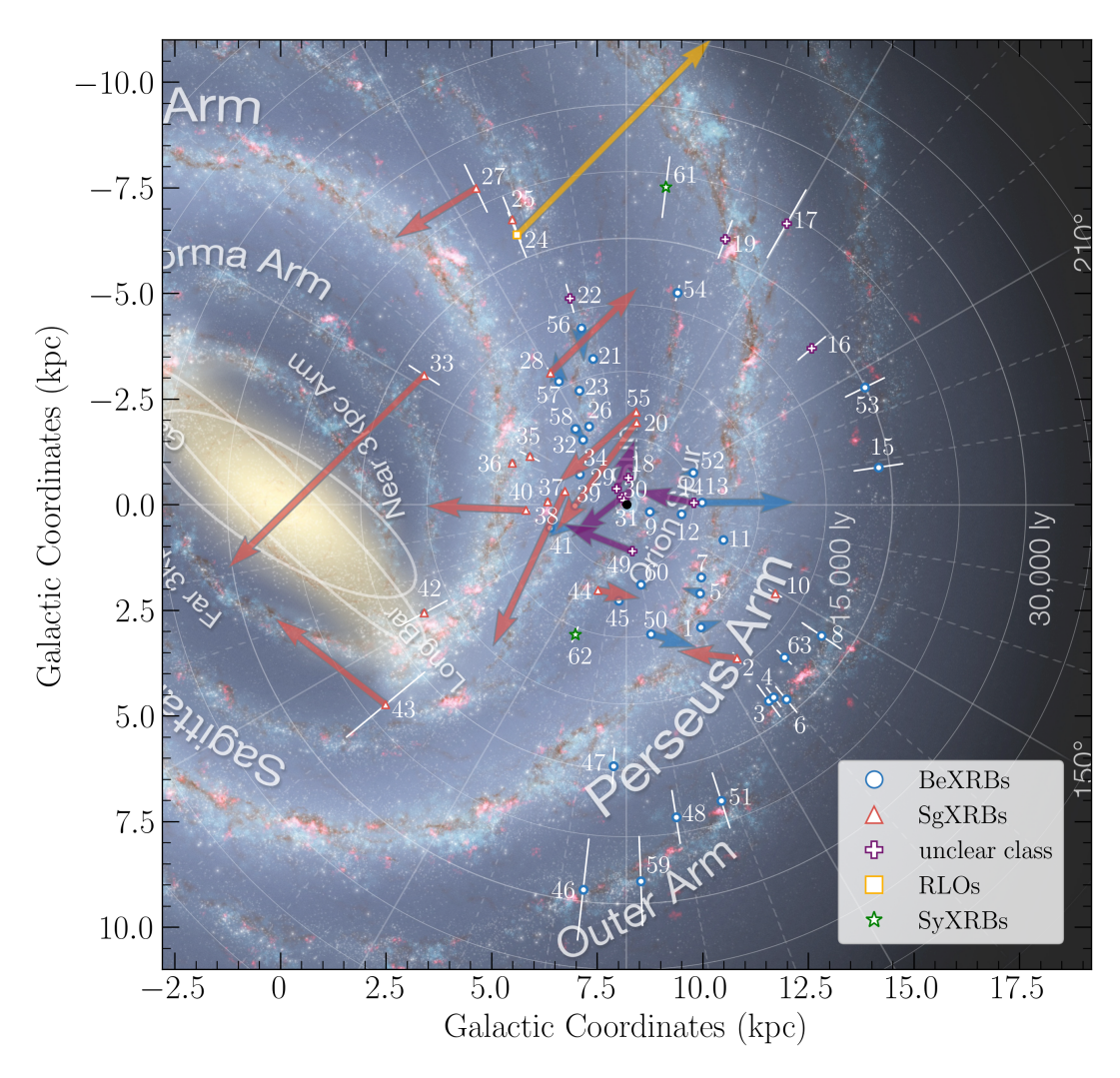
Figure 9. A map of the Galactic plane with the projected locations of 63 HMXBs, incorporating their distance uncertainties accounted for through error propagation (Milky Way image courtesy of NASA/JPL-Caltech, ESO, J. Hurt). The blue dots represent BeXRBs, red dots represent SgXRBs, yellow dot represents RLOs, magenta dots represent unclear classes, green dots represent SyXRBs, and the black dot at the centre is the Sun. The length and direction of the arrows indicate $V_{\rm pec,2D}$ on UV plane ($V_{\rm pec}$ projected on the Galactic plane) for 28 systems with available $V_{\rm r}$ estimates. Numeric labels correspond to system numbers listed in the accompanying table.

period, and systemic $V_{\rm pec}$) and, therefore, are able to estimate any key parameter of interest across the simulated ensemble.

We note that some binaries are consistent with a broad range of pre-SN characteristics, and are sensitive to the natal kick prescriptions implemented. Conversely, in some instances, factors such as mass loss can be tightly constrained. By simulating a large ensemble of $> 10^5$ systems, our methodology averages over the spread introduced by differing evolutionary pathways and unknown starting conditions. We can then use the distributions of physical parameters for successful simulations to extract the mean estimates of the likely pre-SN orbital periods and fractional mass-loss of progenitor stars for our XRBs.

Fig. 10 illustrates the correlation between the mean pre-SN orbital period and fractional mass loss of the simulations for each of the plotted systems. There is a clear separation in how the classes are distributed between these parameters. The majority of SgXRBs systems favour shorter pre-SN orbital periods, with a mean value of 4.0 days, and higher fractional mass loss, with a mean value of 0.5, compared to BeXRBs systems, which have mean values of

172.5 days and 0.3, respectively. These results, albeit preliminary, are aligned with the hypothesis propounded by van den Heuvel et al. (2000) to explain the differences of the peculiar velocities between the classes. Further tests of this scenario should come from developing detailed stellar evolutionary calculations with MESA (Paxton et al. 2015). Updated astrometry from *Gaia*'s new data releases (DR4, 5) in the future should also increase the sample of XRBs with robust kinematic measurements.

6.4 Completeness and Selection Effects

According to Neumann et al. (2023), there are currently 172 known HMXBs. Of these, 151 HMXBs have identified *Gaia* counterparts, but only 63 meet the stringent astrometric criteria set by Bailer-Jones (2015). Consequently, the derived peculiar velocity ($V_{\rm pec}$) values represent only 36 per cent of the confirmed HMXBs in our Galaxy, highlighting the potential impact of selection effects. In particular, the uncertainties in *Gaia* parallax measurements increase towards fainter magnitudes, ranging from 0.02–0.03 mas for $\mathsf{G} < 15$ to 0.07
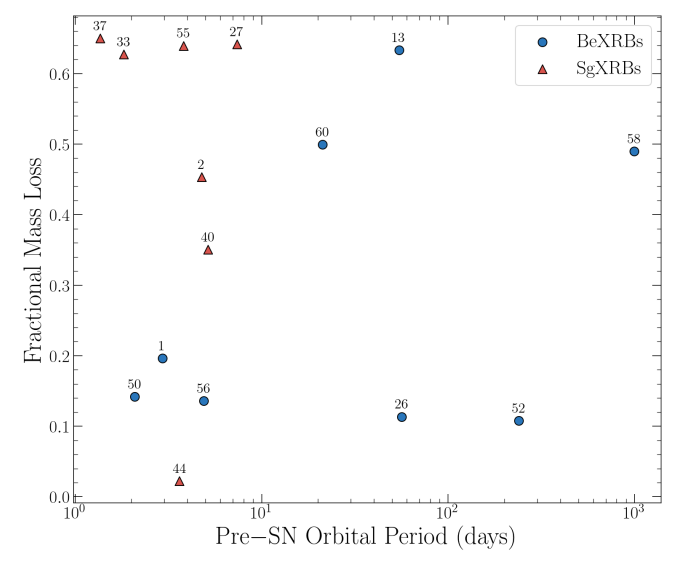
Figure 10. The relationship between pre-SN orbital period and fractional mass loss, based on our binary population synthesis simulations. Systems are distinguished by colour according to sub-classes: blue for BeXRBs, red for SgXRBs. Individual systems are annotated with their corresponding numbers from the Table.

mas at G = 17 and 0.5 mas at G = 20 (Gaia Collaboration 2023). Since our primary astrometric selection criterion is $\pi/\sigma_\pi > 5$, this effectively imposes an absolute-magnitude-dependent flux limit on our sample.

In order to assess the potential impact of such selection effects on our sample, we present the colour-magnitude diagram (CMD) in Fig. 11. Here, systems included in our sample are plotted with filled symbols, while the unfilled symbols show systems with *Gaia* counterparts in the XRBcats catalogue from Neumann et al. (2023). Sub-groups are distinguished with different symbols: circles for BeXRBs, triangles for SgXRBs, plus signs for unclear classifications, squares for RLOs, and stars for SyXRBs. Extinction was accounted for in the plot, and systems without available extinction (A_G) and colour excess values ($E(Bp - Rp)$) were excluded. The grey background dots represent 200,000 stars from the Gaia DR3 archive within 100 pc of the Sun, selected following Gaia Collaboration (2018). Unsurprisingly, the optical counterparts of HMXBs typically occupy the bright and blue region in the CMD parameter space, given the early-type spectral classification of most systems. The CMD suggests that, if there is a systematic bias due to our sample selection, it seems to affect only the intrinsically faintest and reddest systems in XRBcats.

We can further examine the potential impact of selection effects by comparing the 1-D distributions in absolute magnitude and colour for our sample vs those for the XRBcats parent sample (see histograms at the top and right of Fig. 11). No obvious differences are apparent between the two samples. We also construct an independent 'control' sample of 32 sources (unfilled symbols in Fig. 11) by retaining only those sources we are *missing* from XRBcats. We then *quantitively* compare our sample against this control sample via K-S tests on the absolute magnitude and colour distributions. These tests confirm that – for both parameters – the two samples are consistent with being drawn from the same underlying parent distributions. We therefore conclude that our sample should be fairly representative of the *known* HMXB population.

7 SUMMARY

We have investigated the peculiar velocity distribution of Galactic HMXBs by combining data from *Gaia* DR3 with literature V_r estimates. The salient highlights of our work can be summarised as follows:

(i) A search was conducted within a 0.5″ radius in *Gaia* DR3 to identify HMXB candidates, resulting in the detection of optical counterparts for a total of 63 systems with a maximum of parallax uncertainty threshold of 20 per cent. These systems have G-band magnitudes ranging over 6 and 14, and are predominantly located close to the Galactic plane.

(ii) The distribution of estimated distances based on *Gaia* parallaxes agrees with that based on literature distances, albeit with some scatter. No obvious trend or bias in distance estimates is found as a function of source class or astrometric fit quality.

(iii) The V_{pec} distribution is broad, with a mean velocity of ≈ 29 km s^{-1} and maximum values extending up to ≈ 100 km s^{-1}. The mean V_{pec} for BeXRB and SgXRB sub-groups are estimated to be 20.2 km s^{-1} and 48.9 km s^{-1}, respectively. Accounting for the scatter of stellar velocities in the background Galactic disc is expected to moderates these V_{pec} estimates, but will not impact the inference of a kinematic segregation between the source classes.

(iv) The overall V_{pec} distribution reveals two kinematically distinct sub-populations, centred around ≈ 40 km s^{-1}. The low-velocity sub-population is predominantly associated with BeXRBs, while the high-velocity sub-population corresponds to SgXRBs.

(v) The two SyXRBs within the HMXB population exhibit significantly different V_{pec} values from one another, indicating potentially distinct evolutionary paths. Due to the limited sample size of SyXRBs, a deeper understanding of this sub-class requires further investigation.

(vi) The cumulative distribution functions (CDFs) of V_{pec} for BeXRBs and SgXRBs show clear differences, suggesting a preference for lower V_{pec} values in BeXRB systems compared to SgXRBs. A K-S test confirms that the two sub-groups are drawn from statistically distinct distributions.

(vii) For systems with neutron star accretors, V_{pec}-based classifications (BeXRBs: $V_{pec} < 40$ km s^{-1}; SgXRBs: $V_{pec} > 40$ km s^{-1}) are broadly consistent with the location of these classes in the Corbet diagram.

(viii) A test of the directionality of peculiar motions shows that the V_{pec} vectors of HMXBs are consistent with isotropy. The ratio $\langle V_{pec,3D} \rangle / \langle V_{pec,2D} \rangle$ for our sample closely matches the theoretical value of $4/\pi$, enabling reliable estimation of 3D space velocities from observed 2D motions.

(ix) A plausible explanation for the kinematic segration is the differing nature of the progenitor systems for Sg vs. Be systems at the instant of supernova, with correspondingly different orbital velocities and ejecta masses (higher in both respects for the SgXRBs).

(x) Simulations of XRB progenitor systems should be able to test the above scenario, and we utilise population synthesis tests to confirm that SgXRBs systems generally form with shorter pre-SN orbital periods and higher fractional mass loss than BeXRBs systems, supporting the observational trends.

(xi) Irrespective of its physical cause, our empirical results imply that the magnitude of peculiar velocities could potentially be used as a complementary feature for identifying unclassified HMXBs.

(xii) Our result represents 36 per cent of the confirmed HMXB population in our Galaxy. Despite potential selection effects due to parallax uncertainties and sample completeness, comparisons of absolute magnitude and colour distributions, supported by K-S tests, suggest
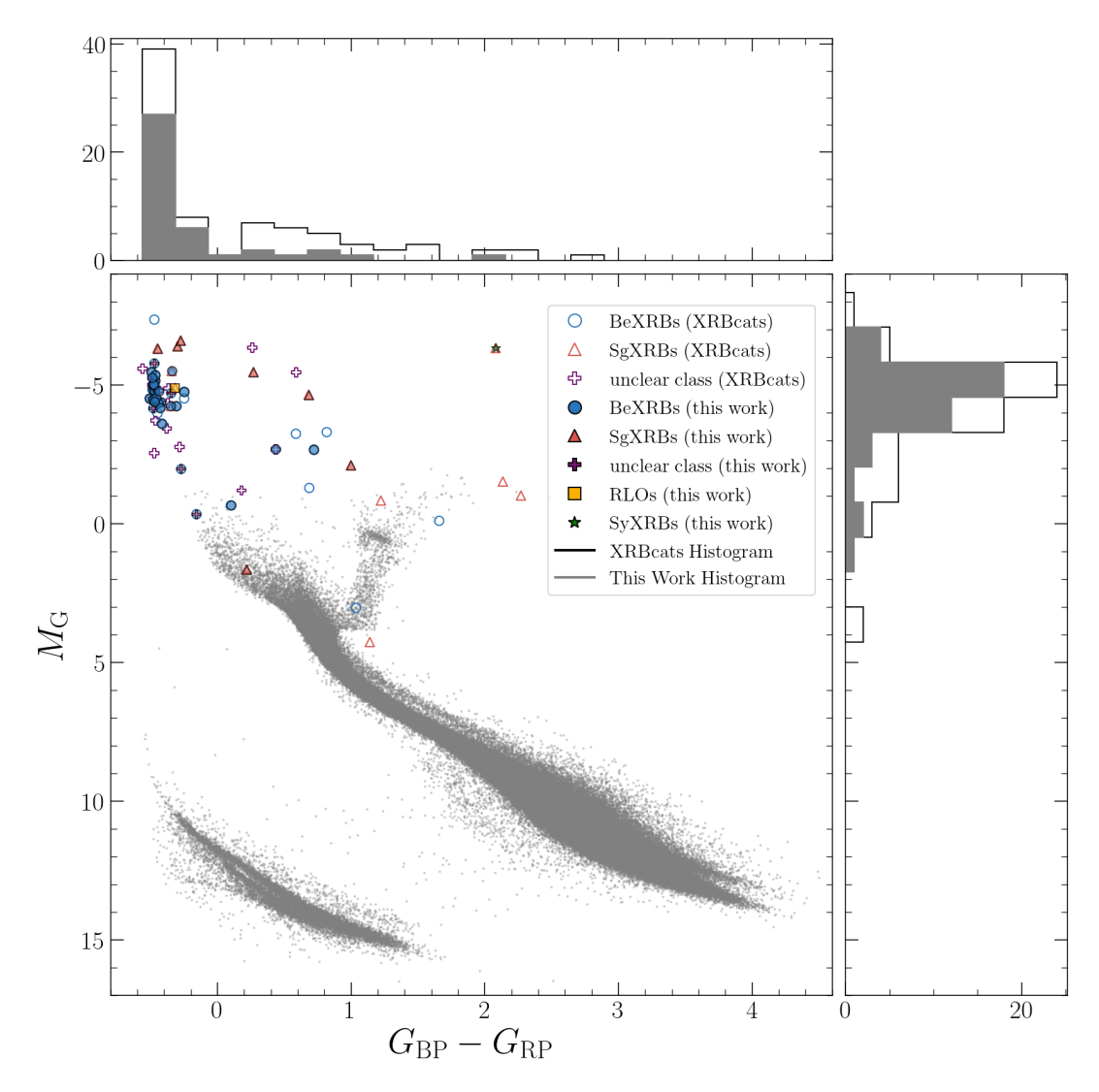
Figure 11. The colour-magnitude diagram (CMD) for HMXBs, where our targets are shown as filled symbols and XRBcats (Neumann et al. 2023) as unfilled symbols. Sub-groups are represented as follows: circles for BeXRBs, triangles for SgXRBs, plus signs for unclear classifications, squares for RLOs, and stars for SyXRBs. Extinction and reddening corrections were applied, where available). The grey background dots represent 200,000 stars queried from the Gaia DR3 archive within 100 pc of the Sun (Gaia Collaboration 2018). The top and right panels show histograms of absolute magnitude $M_{\rm G}$ and colour index $G_{\rm BP} - G_{\rm RP}$, respectively, comparing our targets (filled histograms) with XRBcats (unfilled histograms).

that our sample of 63 systems is representative of the 172 known HMXBs.

DATA AVAILABILITY

The *Gaia* astrometry data can be accessed by querying the Gaia archive. The calculated $V_{\rm pec}$ values will be made available upon reasonable request to the corresponding author.

REFERENCES

Abt H. A., Bautz L. P., 1963, ApJ, 138, 1002
Abubekerov M. K., Antokhina E. A., Cherepashchuk A. M., 2004, Astron. Rep., 48, 89
Aleksić J., et al., 2015, A&A, 576, A36
An H., et al., 2015, ApJ, 806, 166

Ankay A., Kaper L., de Bruijne J. H. J., Dewi J., Hoogerwerf R., Savonije G. J., 2001, A&A, 370, 170

Aragona C., McSwain M. V., Grundstrom E. D., Marsh A. N., Roettenbacher R. M., Hessler K. M., Boyajian T. S., Ray P. S., 2009, ApJ, 698, 514

Aragona C., McSwain M. V., De Becker M., 2010, ApJ, 724, 306

Arras P., Lai D., 1999, Phys. Rev. D, 60, 043001

Atri P., et al., 2019, MNRAS, 489, 3116

Bahramian A., Kennea J. A., Shaw A. W., 2017, The Astronomer's Telegram, 10866, 1

Bailer-Jones C. A. L., 2015, PASP, 127, 994

Barsukova E. A., Borisov N. V., Burenkov A. N., Klochkova V. G., Goranskij V. P., Metlova N. V., 2005, The Astronomer's Telegram, 416, 1

Baykal A., Stark M. J., Swank J., 2000, ApJ, 544, L129

Baykal A., Kızıloğlu Ü., Kızıloğlu N., Balman Ş., Inam S. Ç., 2005, A&A, 439, 1131

Becker R. H., Swank J. H., Boldt E. A., Holt S. S., Pravdo S. H., Saba J. R., Serlemitsos P. J., 1977, ApJ, 216, L11

Belokurov V., et al., 2020, MNRAS, 496, 1922

Bikmaev I. F., et al., 2017, Astronomy Letters, 43, 664

Bird A. J., et al., 2016, ApJS, 223, 15

Blaauw A., 1961, Bull. Astron. Inst. Netherlands, 15, 265

Blay P., Negueruela I., Reig P., Coe M. J., Corbet R. H. D., Fabregat J., Tarasov A. E., 2006, A&A, 446, 1095

Blundell K. M., Bowler M. G., 2004, ApJ, 616, L159

Blundell K. M., Bowler M. G., Schmidtobreick L., 2008, ApJ, 678, L47

Bonnet-Bidaud J.-M., Mouchet M., 1998, A&A

Bonnet-Bidaud J. M., van der Klis M., 1981, A&A, 101, 299

Bozzo E., Romano P., Ferrigno C., Oskinova L., 2022, MNRAS, 513, 42

Breivik K., et al., 2020, ApJ, 898, 71

Carlberg R. G., Dawson P. C., Hsu T., Vandenberg D. A., 1985, ApJ, 294, 674

Casares J., Ribas I., Paredes J. M., Martí J., Allende Prieto C., 2005a, Monthly Notices of the Royal Astronomical Society, 360, 1105

Casares J., Ribó M., Ribas I., Paredes J. M., Martí J., Herrero A., 2005b, MNRAS, 364, 899

Casares J., et al., 2011, in Torres D. F., Rea N., eds, Astrophysics and Space Science Proceedings Vol. 21, High-Energy Emission from Pulsars and their Systems. pp 559–562 (arXiv:1012.4351), doi:10.1007/978-3-642-17251-9_46

Casares J., Ribó M., Ribas I., Paredes J. M., Vilardell F., Negueruela I., 2012, MNRAS, 421, 1103

Casares J., Negueruela I., Ribó M., Ribas I., Paredes J. M., Herrero A., Simón-Díaz S., 2014, Nature, 505, 378

Chevalier C., Ilovaisky S. A., 1998, A&A, 330, 201

Chojnowski S. D., et al., 2017, AJ, 153, 174

Chugai N. N., 1984, Soviet Astronomy Letters, 10, 87

Clark G. W., 2004, ApJ, 610, 956

Clark J. S., et al., 2001, A&A, 376, 476

Clark D. J., et al., 2010, MNRAS, 406, L75

Coe M., Everall C., Norton A., Roche P., Unger S., Fabregat J., Reglero V., Grunsfeld J., 1993, MNRAS, 261, 599

Coe M. J., et al., 1994, MNRAS, 270, L57

Coe M. J., Fabregat J., Negueruela I., Roche P., Steele I. A., 1996, MNRAS, 281, 333

Coleiro A., Chaty S., 2013, ApJ, 764, 185

Corbet R. H. D., 1986, MNRAS, 220, 1047

Corbet R. H. D., Krimm H. A., 2010, The Astronomer's Telegram, 3079, 1

Corbet R. H. D., Mason K. O., 1984, A&A, 131, 385

Corbet R. H. D., Peele A. G., 1997, ApJ, 489, L83

Corbet R. H. D., Peele A. G., 2000, ApJ, 530, L33

Corbet R. H. D., Markwardt C. B., Tueller J., 2007, ApJ, 655, 458

Crampton D., Hutchings J. B., 1981, ApJ, 251, 604

Crampton D., Hutchings J. B., Cowley A. P., 1985, ApJ, 299, 839

Cusumano G., Maccarone M. C., Nicastro L., Sacco B., Kaaret P., 2000, ApJ, 528, L25

Cusumano G., Segreto A., La Parola V., Masetti N., D'Ai A., Tagliaferri G., 2013, MNRAS, 436, L74

Cusumano G., La Parola V., Segreto A., D'Aì A., 2016, MNRAS, 456, 2717

D'Odorico S., Oosterloo T., Zwitter T., Calvani M., 1991, Nature, 353, 329

Dashwood Brown C., Gandhi P., Zhao Y., 2024, MNRAS, 527, L82

Davison P. J. N., Watson M. G., Pye J. P., 1977, MNRAS, 181, 73

De K., Daly F. A., Soria R., 2024, MNRAS, 528, L38

Delgado-Martí H., Levine A. M., Pfahl E., Rappaport S. A., 2001, ApJ, 546, 455

Dominik M., Belczynski K., Fryer C., Holz D. E., Berti E., Bulik T., Mandel I., O'Shaughnessy R., 2012, ApJ, 759, 52

Dorofeev O. F., Rodionov V. N., Ternov I. M., 1985, Soviet Astronomy Letters, 11, 123

Doroshenko V., Tsygankov S., Santangelo A., 2018, A&A, 613, A19

Drave S. P., Clark D. J., Bird A. J., McBride V. A., Hill A. B., Sguera V., Scaringi S., Bazzano A., 2010, MNRAS, 409, 1220

Ducci L., Doroshenko V., Suleimanov V., Nikołajuk M., Santangelo A., Ferrigno C., 2016, A&A, 592, A58

Duflot M., Figon P., Meyssonnier N., 1995, A&AS, 114, 269

ESA ed. 1997, The HIPPARCOS and TYCHO catalogues. Astrometric and photometric star catalogues derived from the ESA HIPPARCOS Space Astrometry Mission ESA Special Publication Vol. 1200

Fabregat J., et al., 1992, A&A, 259, 522

Fairlamb J. R., Oudmaijer R. D., Mendigutía I., Ilee J. D., van den Ancker M. E., 2015, MNRAS, 453, 976

Falanga M., Bozzo E., Lutovinov A., Bonnet-Bidaud J. M., Fetisova Y., Puls J., 2015, A&A, 577, A130

Ferrigno C., Farinelli R., Bozzo E., Pottschmidt K., Klochkov D., Kretschmar P., 2013, A&A, 553, A103

Finger M. H., Ikhsanov N. R., Wilson-Hodge C. A., Patel S. K., 2010, ApJ, 709, 1249

Forman W., Jones C., Cominsky L., Julien P., Murray S., Peters G., Tananbaum H., Giacconi R., 1978, ApJS, 38, 357

Fornasini F. M., Antoniou V., Dubus G., 2023, arXiv e-prints, p. arXiv:2308.02645

Fortin F., Garcia F., Chaty S., Chassande-Mottin E., Bunzel A. S., 2022, A&A

Fortin F., García F., Simaz Bunzel A., Chaty S., 2023, A&A, 671, A149

Frail D. A., Hjellming R. M., 1991, AJ, 101, 2126

Fryer C. L., Kalogera V., 2001, ApJ, 554, 548

Fryer C. L., Belczynski K., Wiktorowicz G., Dominik M., Kalogera V., Holz D. E., 2012, ApJ, 749, 91

Gaia Collaboration 2016, A&A, 595, A1

Gaia Collaboration 2018, A&A, 616, A10

Gaia Collaboration 2023, A&A, 674, A1

Gamen R., Barbà R. H., Walborn N. R., Morrell N. I., Arias J. I., Maíz Apellániz J., Sota A., Alfaro E. J., 2015a, A&A, 583, L4

Gamen R., Barbà R. H., Walborn N. R., Morrell N. I., Arias J. I., Maíz Apellániz J., Sota A., Alfaro E. J., 2015b, A&A, 583, L4

Gandhi P., Rao A., Johnson M. A. C., Paice J. A., Maccarone T. J., 2019, MNRAS, 485, 2642

Gandhi P., Rao A., Charles P. A., Belczynski K., Maccarone T. J., Arur K., Corral-Santana J. M., 2020, MNRAS: Letters, 496, L22

Gandhi P., et al., 2022, MNRAS, 510, 3885

Gies D. R., Bolton C. T., 1982, ApJ, 260, 240

Gies D. R., Bolton C. T., 1986, ApJS, 61, 419

Gies D. R., et al., 2003, ApJ, 583, 424

Gies D. R., et al., 2008, ApJ, 678, 1237

González-Galán A., Negueruela I., Castro N., Simón-Díaz S., Lorenzo J., Vilardell F., 2014, A&A, 566, A131

González-Riestra R., Oosterbroek T., Kuulkers E., Orr A., Parmar A. N., 2004, A&A, 420, 589

Goossens M. E., Bird A. J., Drave S. P., Bazzano A., Hill A. B., McBride V. A., Sguera V., Sidoli L., 2013, MNRAS, 434, 2182

Gregory P. C., 2002, ApJ, 575, 427

Grillo F., Sciortino S., Micela G., Vaiana G. S., Harnden Jr. F. R., 1992, ApJS, 81, 795

Groenewegen M., 2021, A&A, 654, A20

Gromadzki M., Mikołajewska J., Soszyński I., 2013, Acta Astron., 63, 405

Grundstrom E. D., et al., 2007, ApJ, 660, 1398

Grunhut J. H., Bolton C. T., McSwain M. V., 2014, A&A, 563, A1

Haberl F., Angelini L., Motch C., 1998, A&A, 335, 587

Hambaryan V., et al., 2022, MNRAS, 511, 4123

Hillwig T. C., Gies D. R., Huang W., McSwain M. V., Stark M. A., van der Meer A., Kaper L., 2004, ApJ, 615, 422

Hinkle K. H., Lebzelter T., Fekel F. C., Straniero O., Joyce R. R., Prato L., Karnath N., Habel N., 2020, ApJ, 904, 143

Hobbs G., Lorimer D. R., Lyne A. G., Kramer M., 2005, MNRAS, 360, 974

Hu C.-P., Chou Y., Ng C. Y., Lin L. C.-C., Yen D. C.-C., 2017, ApJ, 844, 16

Hutchings J. B., 1984, Publications of the Astronomical Society of the Pacific, 96, 312

Hutchings J., Cowley A., Crampton D., Paradus J., White N., 1979, ApJ, 229

Hutchings J., Crampton D., Cowley A., 1981, AJ, 86, 871

Hutchings J. B., Crampton D., Cowley A. P., Thompson I. B., 1987, PASP, 99, 420

Ilovaisky S. A., Chevalier C., Motch C., 1982, A&A, 114, L7

Janka H.-T., 2017, ApJ, 837, 84

Janot-Pacheco E., Ilovaisky S. A., Chevalier C., 1981, A&A, 99, 274

Janssens S., Shenar T., Degenaar N., Bodensteiner J., Sana H., Audenaert J., Frost A. J., 2023, A&A, 677, L9

Jaschek M., Jaschek C., 1963, PASP, 75, 365

Jenke P., Wilson-Hodge C. A., 2017, The Astronomer's Telegram, 10812, 1

Johnston M., Bradt H., Doxsey R., Gursky H., Schwartz D., Schwarz J., 1978, ApJ, 223, L71

Johnston S., Manchester R. N., Lyne A. G., Nicastro L., Spyromilio J., 1994, MNRAS, 268, 430

Jones C., Forman W., Tananbaum H., Schreier E., Gursky H., Kellogg E., Giacconi R., 1973, ApJ, 181, L43

Jönsson H., et al., 2020, AJ, 160, 120

Kaaret P., Cusumano G., Sacco B., 2000, ApJ, 542, L41

Kalogera V., 1996, ApJ, 471, 352

Kaper L., Lamers H. J. G. L. M., Ruymaekers E., Heuvel E. P. J. v. d., Zuiderwijk E. J., 1995, A&A

Kaper L., van der Meer A., Najarro F., 2006, A&A, 457, 595

Karasev D. I., Lutovinov A. A., Burenin R. A., 2010, MNRAS, 409, L69

Kaur R., Paul B., Kumar B., Sagar R., 2008, MNRAS, 386, 2253

Kawata D., Bovy J., Matsunaga N., Baba J., 2019, MNRAS, 482, 40

Kelley R. L., Rappaport S., Clark G. W., Petro L. D., 1983, ApJ, 268, 790

Kennea J. A., Lien A. Y., Krimm H. A., Cenko S. B., Siegel M. H., 2017, The Astronomer's Telegram, 10809, 1

Kharchenko N. V., Scholz R.-D., Piskunov A. E., Röser S., Schilbach E., 2007, Astronomische Nachrichten, 328, 889

Knigge C., Coe M. J., Podsiadlowski P., 2011, Nature, 479, 372

Koenigsberger G., Canalizo G., Arrieta A., Richer M. G., Georgiev L., 2003, Revista Mexicana de Astronomia y Astrofisica, 39, 17

Kouroubatzakis K., Reig P., Andrews J.,) A. Z., 2017, The Astronomer's Telegram, 10822, 1

Koyama K., et al., 1991, ApJ, 366, L19

LaSala J., Charles P. A., Smith R. A. D., Balucinska-Church M., Church M. J., 1998, MNRAS, 301, 285

Lamb R. C., Markert T. H., Hartman R. C., Thompson D. J., Bignami G. F., 1980, ApJ, 239, 651

Leahy D. A., 2002, A&A, 391, 219

Leyder J.-C., Walter R., Lazos M., Masetti N., Produit N., 2007, A&A, 465, L35

Lindegren L., Bastian U., 2010, in EAS Publications Series. pp 109–114, doi:10.1051/eas/1045018

Lindegren L., et al., 2021, A&A, 649, A4

Liu Q. Z., van Paradijs J., van den Heuvel E. P. J., 2006, A&A, 455, 1165

Luna G. J. M., Sokoloski J. L., 2007, ApJ, 671, 741

Lutovinov A., Revnivtsev M., Gilfanov M., Shtykovskiy P., Molkov S., Sunyaev R., 2005, A&A, 444, 821

Lyubimkov L. S., Rostopchin S. I., Roche P., Tarasov A. E., 1997, MNRAS, 286, 549

Lyuty V. M., Zaĭtseva G. V., 2000, Astronomy Letters, 26, 9

Manchester R. N., Johnston S., Lyne A. G., D'Amico N., Bailes M., Nicastro L., 1995, ApJ, 445, L137

Marcote B., Ribó M., Paredes J. M., Mao M. Y., Edwards P. G., 2018, A&A, 619, A26

Masetti N., Orlandini M., Palazzi E., Amati L., Frontera F., 2006a, A&A, 453, 295

Masetti N., et al., 2006b, A&A, 455, 11

Masetti N., et al., 2009, A&A, 495, 121

Masetti N., et al., 2012, A&A, 538, A123

McBride V. A., et al., 2006, A&A, 451, 267

McBride V. A., et al., 2007, A&A, 470, 1065

McSwain M. V., Gies D. R., Riddle R. L., Wang Z., Wingert D. W., 2001, ApJ, 558, L43

McSwain M. V., Gies D. R., Huang W., Wiita P. J., Wingert D. W., Kaper L., 2004, ApJ, 600, 927

Mereghetti S., La Palombara N., 2009, A&A, 504, 181

Middleton M. J., et al., 2021, MNRAS, 506, 1045

Miller-Jones J. C. A., et al., 2018, MNRAS, 479, 4849

Miller-Jones J. C. A., et al., 2021, Science, 371, 1046

Mirabel F., 2017, New Astron. Rev., 78, 1

Mirabel I. F., Rodrigues I., 2003, Science, 300, 1119

Monageng I. M., McBride V. A., Alfonso-Garzon J., Townsend L. J., Coley J. B., Montesinos B., Corbet R. H. D., Pottschmidt K., 2024, MNRAS, 527, 5293

Moritani Y., Kawano T., Chimasu S., Kawachi A., Takahashi H., Takata J., Carciofi A. C., 2018a, PASJ, 70

Moritani Y., Kawano T., Chimasu S., Kawachi A., Takahashi H., Takata J., Carciofi A. C., 2018b, PASJ, 70, 61

Motch C., Haberl F., Dennerl K., Pakull M., Janot-Pacheco E., 1997, A&A, 323, 853

Murakami T., Kawai N., Makishima K., Mitani K., Hayakawa S., Nagase F., Tawara Y., Kunieda H., 1984, PASJ, 36, 691

Nagase F., 1989, PASJ, 41, 1

Negueruela I., 1998, A&A, 338, 505

Negueruela I., 2010, in Martí J., Luque-Escamilla P. L., Combi J. A., eds, Astronomical Society of the Pacific Conference Series Vol. 422, High Energy Phenomena in Massive Stars. p. 57 (arXiv:0907.2883), doi:10.48550/arXiv.0907.2883

Negueruela I., Okazaki A. T., 2001, A&A, 369, 108

Negueruela I., Roche P., Buckley D. a. H., Chakrabarty D., Coe M. J., Fabregat J., Reig P., 1996, A&A, 315, 160

Negueruela I., Roche P., Fabregat J., Coe M. J., 1999, MNRAS, 307, 695

Negueruela I., Smith D. M., Chaty S., 2005, The Astronomer's Telegram, 470, 1

Negueruela I., Smith D. M., Harrison T. E., Torrejon J. M., 2006, ApJ, 638, 982

Nelemans G., Tauris T. M., van den Heuvel E. P. J., 1999, A&A, 352, L87

Neumann M., Avakyan A., Doroshenko V., Santangelo A., 2023, A&A, 677, A134

Nikolaeva E. A., Bikmaev I. F., Melnikov S. S., Galeev A. I., Zhuchkov R. Y., Irtuganov E. N., 2013, Bulletin Crimean Astrophysical Observatory, 109, 27

Okazaki A. T., Negueruela I., 2001, A&A, 377, 161

Paredes-Fortuny X., Ribó M., Fors O., Núñez J., 2012, in Aharonian F. A., Hofmann W., Rieger F. M., eds, American Institute of Physics Conference Series Vol. 1505, High Energy Gamma-Ray Astronomy: 5th International Meeting on High Energy Gamma-Ray Astronomy. pp 390–393 (arXiv:1210.1151), doi:10.1063/1.4772279

Parkes G. E., Murdin P. G., Mason K. O., 1980a, MNRAS, 190, 537

Parkes G. E., Mason K. O., Murdin P. G., Culhane J. L., 1980b, MNRAS, 191, 547

Paxton B., et al., 2015, ApJS, 220, 15

Pellizza L. J., Chaty S., Negueruela I., 2006, A&A, 455, 653

Picchi P., Shore S. N., Harvey E. J., Berdyugin A., 2020, A&A, 640, A96

Polcaro V. F., et al., 1989, in Hunt J., Battrick B., eds, ESA Special Publication Vol. 1, Two Topics in X-Ray Astronomy, Volume 1: X Ray Binaries. Volume 2: AGN and the X Ray Background. p. 579

Priedhorsky W. C., Terrell J., 1983a, ApJ, 273, 709

Priedhorsky W. C., Terrell J., 1983b, Nature, 303, 681

Rao A., Gandhi P., Knigge C., Paice J. A., Leigh N. W. C., Boubert D., 2020a, MNRAS, 495, 1491

Rao A., Gandhi P., Knigge C., Paice J. A., Leigh N. W. C., Boubert D., 2020b, MNRAS, 495, 1491

Rappaport S., Clark G. W., Cominsky L., Joss P. C., Li F., 1978, ApJ, 224, L1

Ray P. S., Chakrabarty D., 2002, ApJ, 581, 1293

Reid M. J., et al., 2009, ApJ, 700, 137

Reid M. J., McClintock J. E., Narayan R., Gou L., Remillard R. A., Orosz J. A., 2011, ApJ, 742, 83

Reig P., Fabregat J., 2015, A&A, 574, A33

Reig P., Roche P., 1999a, MNRAS, 306, 95

Reig P., Roche P., 1999b, MNRAS, 306, 100

Reig P., Zezas A., 2018, A&A, 613, A52

Reig P., Chakrabarty D., Coe M. J., Fabregat J., Negueruela I., Prince T. A., Roche P., Steele I. A., 1996, A&A, 311, 879

Reig P., Fabregat J., Coe M. J., Roche P., Chakrabarty D., Negueruela I., Steele I., 1997, A&A, 322, 183

Reig P., Negueruela I., Buckley D. A. H., Coe M. J., Fabregat J., Haigh N. J., 2001, A&A, 367, 266

Reig P., Negueruela I., Fabregat J., Chato R., Blay P., Mavromatakis F., 2004, A&A, 421, 673

Reig P., Negueruela I., Papamastorakis G., Manousakis A., Kougentakis T., 2005a, A&A, 440, 637

Reig P., Negueruela I., Fabregat J., Chato R., Coe M. J., 2005b, A&A, 440, 1079

Reig P., Zezas A., Gkouvelis L., 2010, A&A, 522, A107

Reig P., Nersesian A., Zezas A., Gkouvelis L., Coe M. J., 2016, A&A, 590, A122

Reig P., Fabregat J., Alfonso-Garzón J., 2020, A&A, 640, A35

Renzo M., et al., 2019, A&A, 624, A66

Repetto S., Igoshev A. P., Nelemans G., 2017, MNRAS, p. stx027

Reynolds A. P., Bell S. A., Hilditch R. W., 1992, MNRAS, 256, 631

Rivinius T., Klement R., Chojnowski S. D., Baade D., Shepard K., Hadrava P., 2024, in Mackey J., Vink J. S., St-Louis N., eds, IAU Symposium Vol. 361, IAU Symposium. pp 332–333, doi:10.1017/S1743921322002976

Robinson E. L., Ivans I. I., Welsh W. F., 2002, ApJ, 565, 1169

Romano P., et al., 2015, A&A, 576, L4

Sadakane K., Hirata R., 1985, ApJ, 288, 8

Sarty G. E., et al., 2009, MNRAS, 392, 1242

Sato N., Nagase F., Kawai N., Kelley R. L., Rappaport S., White N. E., 1986, ApJ, 304, 241

Sidoli L., Vercellone S., Mereghetti S., Tavani M., 2005, A&A, 429, L47

Sidoli L., Paizis A., Mereghetti S., 2006, A&A, 450, L9

Sidoli L., Romano P., Mereghetti S., Paizis A., Vercellone S., Mangano V., Götz D., 2007, A&A, 476, 1307

Smith D. M., 2004, The Astronomer's Telegram, 338

Staubert R., Pottschmidt K., Doroshenko V., Wilms J., Suchy S., Rothschild R., Santangelo A., 2011, A&A, 527, A7

Steele I. A., Negueruela I., Coe M. J., Roche P., 1998, MNRAS, 297, L5

Stella L., White N. E., Davelaar J., Parmar A. N., Blissett R. J., van der Klis M., 1985, ApJ, 288, L45

Stevens J. B., Reig P., Coe M. J., Buckley D. A. H., Fabregat J., Steele I. A., 1997, MNRAS, 288, 988

Stickland D. J., Lloyd C., 1994, The Observatory, 114, 41

Stickland D., Lloyd C., Radziun-Woodham A., 1997, MNRAS, 286, L21

Stollberg M. T., Finger M. H., Wilson R. B., Harmon B. A., Rubin B. C., Zhang N. S., Fishman G. J., 1993, IAU Circ., 5836, 1

Stoyanov K. A., Zamanov R. K., Latev G. Y., Abedin A. Y., Tomov N. A., 2014, Astronomische Nachrichten, 335, 1060

Strader J., Chomiuk L., Cheung C. C., Salinas R., Peacock M., 2015a, ApJ, 813, L26

Strader J., Chomiuk L., Cheung C. C., Salinas R., Peacock M., 2015b, ApJ, 813, L26

Swank J. H., Smith D. M., Markwardt C. B., 2007, The Astronomer's Telegram, 999, 1

Thackeray A. D., 1970, MNRAS, 150, 215

Torrejón J. M., Orr A., 2001, A&A, 377, 148

Tsyganov S. S., Doroshenko V., Mushtukov A. A., Lutovinov A. A., Poutanen J., 2018, MNRAS, 479, L134

Tweedy R. W., Warwick R. S., Remillard R., 1989, in Hunt J., Battrick B., eds, ESA Special Publication Vol. 1, Two Topics in X-Ray Astronomy, Volume 1: X Ray Binaries. Volume 2: AGN and the X Ray Background. p. 661

Vink J. S., de Koter A., 2005, A&A, 442, 587

Vink J. S., de Koter A., Lamers H. J. G. L. M., 2001, A&A, 369, 574

Virtanen P., et al., 2020, scipy/scipy: SciPy 1.5.3, Zenodo, doi:10.5281/zenodo.4100507

Volkov I., Kargaltsev O., Younes G., Hare J., Pavlov G., 2021, ApJ, 915, 61

Walter R., Lutovinov A. A., Bozzo E., Tsygankov S. S., 2015, A&ARv, 23, 2

Wang W., 2010, A&A, 516, A15

Wang W., 2011, MNRAS, 413, 1083

Wang X. I., Li X.-D., 2025, ApJ, 985, 12

Waters L. B. F. M., Pols O. R., Hogeveen S. J., Cote J., van den Heuvel E. P. J., 1989, A&A, 220, L1

Williams S. J., Gies D. R., Matson R. A., Touhami Y., Grundstrom E. D., Huang W., McSwain M. V., 2010, ApJ, 723, L93

Wilson R. E., 1953, Carnegie Institute Washington D.C. Publication

Wilson-Hodge C. A., et al., 2018, ApJ, 863, 9

Wilson C. A., Finger M. H., Harmon B. A., Chakrabarty D., Strohmayer T., 1998, ApJ, 499, 820

Yoneda H., Makishima K., Enoto T., Khangulyan D., Matsumoto T., Takahashi T., 2020, Phys. Rev. Lett., 125, 111103

Zeng L., Zhang M., Ren C., Zhang P., Yan J., 2024, ApJ, 977, 40

Zhao Y., Gandhi P., Brown C. D., Knigge C., Charles P. A., Maccarone T. J., Nuchvanichakul P., 2023, MNRAS,

Zorec J., Frémat Y., Cidale L., 2005, A&A, 441, 235

den Hartog P. R., Kuiper L. M., Corbet R. H. D., in't Zand J. J. M., Hermsen W., Vink J., Remillard R., van der Klis M., 2004, The Astronomer's Telegram, 281, 1

in't Zand J. J. M., Halpern J., Eracleous M., McCollough M., Augusteijn T., Remillard R. A., Heise J., 2000, A&A, 361, 85

in't Zand J. J. M., Swank J., Corbet R. H. D., Markwardt C. B., 2001, A&A, 380, L26

in't Zand J. J. M., Kuiper L., den Hartog P. R., Hermsen W., Corbet R. H. D., 2007, A&A, 469, 1063

van den Heuvel E. P. J., Zwart S. F. P., Bhattacharya D., Kaper L., 2000, A&A

van der Klis M., Bonnet-Bidaud J. M., 1984, A&A, 135, 155

van der Meij V., Guo D., Kaper L., Renzo M., 2021, A&A, 655, A31

APPENDIX

7.1 Additional discussion of specific HMXBs

7.1.1 BH systems

Throughout our analyses, we include 4 systems that may host a BH, and some of their classification is still under some debate. In this section, we present individual discussion on these systems.

RX J1826.2–1450/LS 5039: This system is a HMXB first discovered by Motch et al. (1997). Its optical counterpart, LS 5039, is an O star (6.5V((f)), Clark et al. 2001) and is in a 4.4-day orbit with a compact companion (McSwain et al. 2001, 2004). Casares et al. (2005b) reported the mass of the compact object to be $3.7^{+1.3}_{-1.0}$ $M_\odot$, suggesting that the compact object as a BH. Recent studies found signs of X-ray pulsations, so the compact object is more likely a NS (Yoneda et al. 2020; Volkov et al. 2021). Fortin et al. (2022) found the V_{pec} of $89.1^{+2.8}_{-2.6}$ km s^{-1}; our calculation yields a consistent V_{pec} of $90.3^{+3.0}_{-2.9}$ km s^{-1}, making it the fastest BeXRB in our sample. Furthermore, a recent study by Zeng et al. (2024) suggests that LS 5039 may be a triple system, with a third body orbiting the barycentre of the binary. Gravitational interactions, including oscillations or dynamical ejection during close encounters, could alter the system's orbit and explain its high V_{pec}. However,
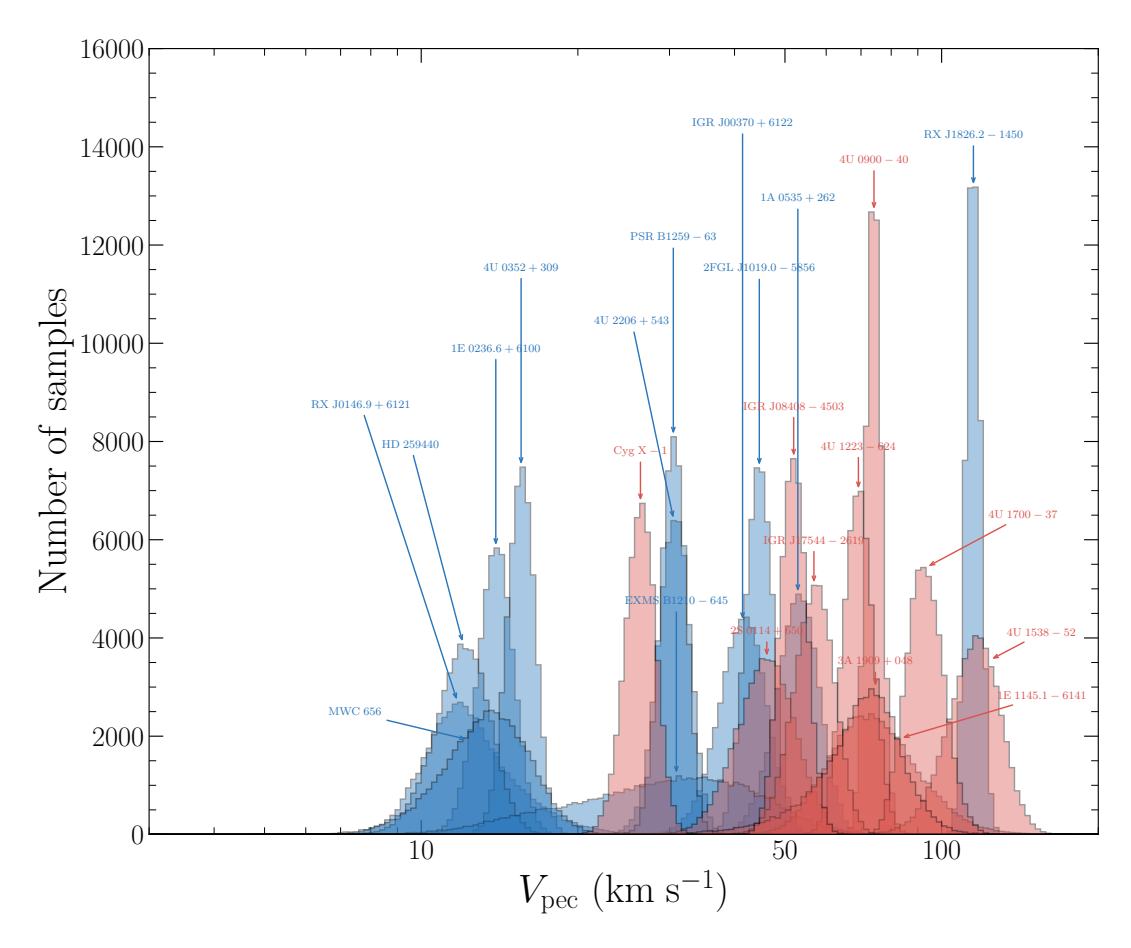
Figure 12. Individual posterior distributions of V_{pec} for BeXRBs (blue) and SgXRBs (red). Only systems with available V_r values are included here. For each source, 50,000 random samples are drawn.

triple systems are not expected to significantly contribute to the high-velocity regime, as such systems typically require tight orbits, whereas the configuration of this system likely involves a third body in a wide orbit.

3A 1909+048/SS 433: This is a well-known HMXB hosting a supergiant and a compact object in an 13.1-day orbit (Crampton & Hutchings 1981). A compact object mass 2.9 $M_\odot$, which suggests that it might be a stellar-mass BH in the mass gap (Hillwig et al. 2004). The nature of the compact object in SS 433 is still under debate. Spectroscopic observations estimating the compact object's orbital speed, combined with the mass ratio from X-ray data, suggested that the compact object is likely a NS (D'Odorico et al. 1991). Its V_{pec} is 57.0±10 km s^{-1}. It is often highlighted as the prototypical Galactic ultra-luminous X-ray source, plausibly a neutron star undergoing super-critical accretion, though this remains under debate (e.g., Blundell et al. 2008; Middleton et al. 2021).

4U 1956+35/Cyg X–1: Cyg X–1 was the first BH HMXB to be identified in X-rays, and is now known to host a BH of approximately 21.2 $M_\odot$ and a O9.7 Iab supergiant with a mass of $\approx M_\odot$ (Miller-Jones et al. 2021) in a close (5.6-day) orbit (Gies et al. 2003). Its V_{pec} 20.8$^{+1.4}_{-1.4}$ km s^{-1}, which is quite low velocity for SgXRBs. This could be attributed to the evolutionary path of Cyg X–1. BH in Cyg X–1 was form by implosion where system may not have experienced an energetic trigger from NK or significant mass loss associated with a SN event (Mirabel & Rodrigues 2003). In this

study, we use the same method applied to other systems to calculate the V_{pec} of Cyg X–1 relative to the Galactic centre. Since Cyg X–1 is associated with the massive star cluster Cygnus OB3 (Mirabel & Rodrigues 2003), which is considered its parent association, the peculiar velocity should ideally be measured relative to Cygnus OB3. Previous studies report a V_{pec} of $\approx 9\pm2$ km s^{-1} relative to Cygnus OB3 (Mirabel & Rodrigues 2003; Rao et al. 2020b). Thus, the V_{pec} we derive here, being relative to the Galactic centre, can be considered as an upper limit.

MWC 656/HD 215227: This is a BeXRB with an orbital period of 60.37±0.04 days (Williams et al. 2010; Paredes-Fortuny et al. 2012; Casares et al. 2012, 2014). Studies of the optical counterpart and spectral type of the secondary suggested a distance of 2.6±0.6 kpc (Casares et al. 2014) and also indicated that the compact object in the system is a BH with a mass of 3.8–6.9 $M_\odot$, making MWC 656 the first known Be/BH system (Casares et al. 2014). However, Rivinius et al. (2024) revisited the spectral variability properties of MWC 656 and concluded that it is more likely to be a hot subdwarf rather than a BH. This conclusion was further supported by Janssens et al. (2023), that the compact object in this system is not a black hole from spectroscopic data with high-Resolution Mercator Echelle Spectrograph (*HERMES*). Similar to other BeXRBs in our sample, MWC 565 has a low V_{pec} (23.9±10 km s^{-1}). Such a low velocity suggests that the BH may have formed through direct collapse, without experiencing a NK from a SN explosion, similar to the case of Cyg X–1.
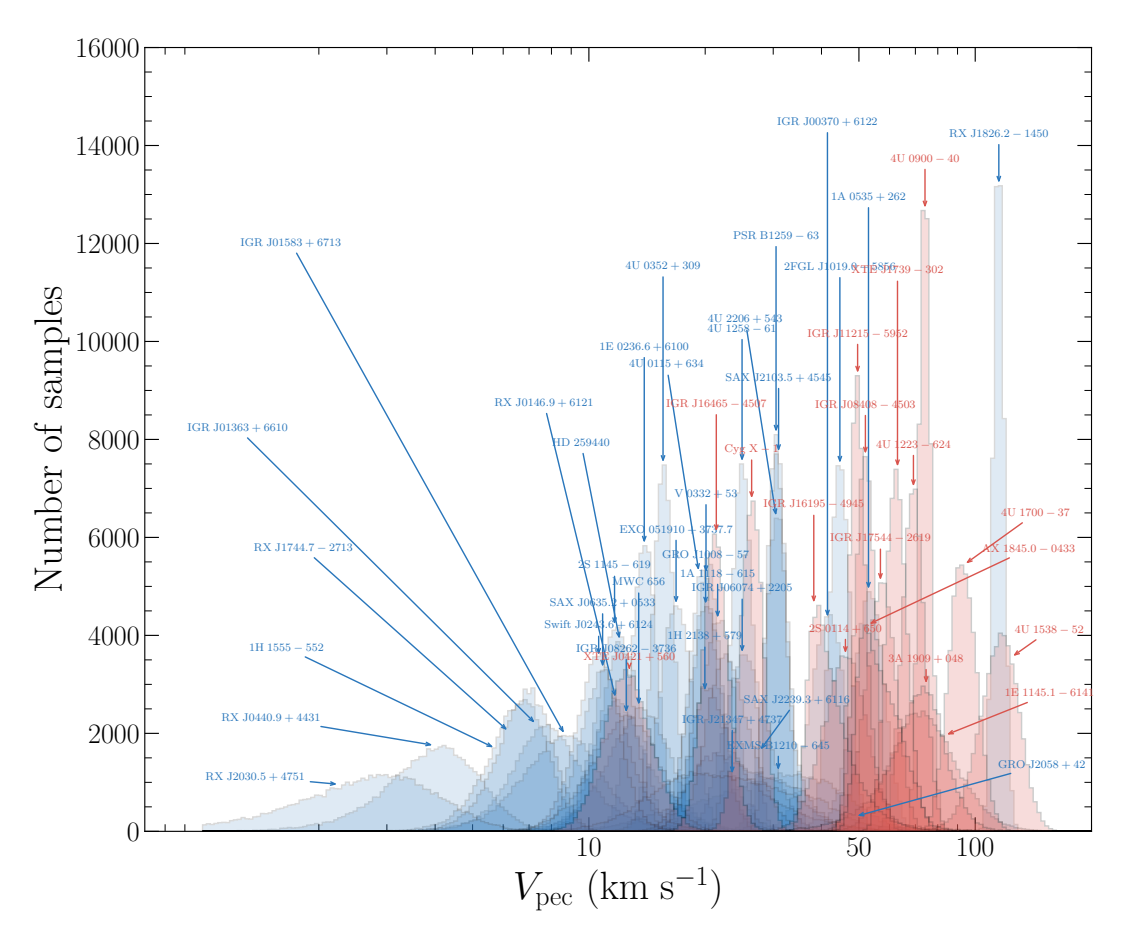
Figure 13. Individual probability distributions of V_{pec} for BeXRBs (blue) and SgXRBs (red). Systems with assumed V_r values using the isotropic assumption are included here. For each source, 50,000 random samples were drawn for plotting the probability distribution.

7.1.2 SyXRBs

We include two rare cases of symbiotic HMXBs in our sample, both with no available V_r measurements. Our calculation reveals substantial different V_{pec}s for these two systems.

4U 1954+31: This system was discovered by the *Uhuru (SAS A)* mission (Forman et al. 1978). The early X-ray position has substantial uncertainty, which encloses multiple counterparts, including a Be star (Tweedy et al. 1989). A significantly more precise position was reported by *Chandra* observations, identifying this system with an M-type star (Masetti et al. 2006a), the spectral type was also confirmed by its near-infrared spectrum (Hinkle et al. 2020). The estimated mass of the donor star is approximately 9^{+6}_{-2} $M_\odot$ (Hinkle et al. 2020). We derive a low V_{pec} of $19.7^{+2.2}_{-2.1}$ km s^{-1}, consistent with a mild kick received at the instant of a supernova. This result supports the assumption of Hinkle et al. (2020), suggesting that the supernova might ablate the surface of the B-type main-sequence companion. Alternatively, the subsequent mixing of surface material into the envelope could have occurred, causing the B-type main-sequence star to evolve into an M supergiant.

Swift J0850.8–4219/2MASS J08504008–4211514: This system was recently discovered by *Swift/XRT* as the second Galactic SyXRB. A possible near-infrared counterpart, 2MASS 08504008–4211514, corresponds to an red supergiant (RSG) of spectral type K3-K5 with an estimated distance of ≈12 kpc (De et al. 2024). This system has a

high V_{pec} of 68.8±19 km s^{-1}. If the companion turns out to be of low mass, this could be explained with a small system inertia, making it less resistant to acceleration by a natal kick and consequently leading to a relatively higher peculiar velocity. But this remains to be tested, as the system is still relatively new and ill-understood at the time of writing.

7.1.3 Promising systems

Swift J0243.6+6124: This system was recently discovered by *Swift/BAT* as the first and, to date, only ULXP identified within our Galaxy (Kennea et al. 2017; Doroshenko et al. 2018; Tsygankov et al. 2018; Wilson-Hodge et al. 2018). Its pulsation period of approximately 9.86 s has been confirmed by observations from *Swift/XRT* (Kennea et al. 2017), *Fermi/GBM* (Jenke & Wilson-Hodge 2017), and *NuSTAR* (Bahramian et al. 2017). Optical spectroscopy initially identified the source as a new BeXRBs (Kouroubatzakis et al. 2017), with subsequent analysis classifying the optical companion as an O9.5Ve star (Reig et al. 2020). Photometric measurements of the optical counterpart suggest a distance of 4.5 ± 0.5 kpc (Reig et al. 2020).

There is only a single published V_r measurement available from SDSS/APOGEE, reporting a notably high value of 325.71 km s^{-1} (Jönsson et al. 2020), which subsequently yields a very large V_{pec} estimate of 393.76 km s^{-1} as reported by Wang & Li (2025). Given the lack of corroborating V_r measurements, the reliability of this single measurement is uncertain. Therefore, we conservatively choose

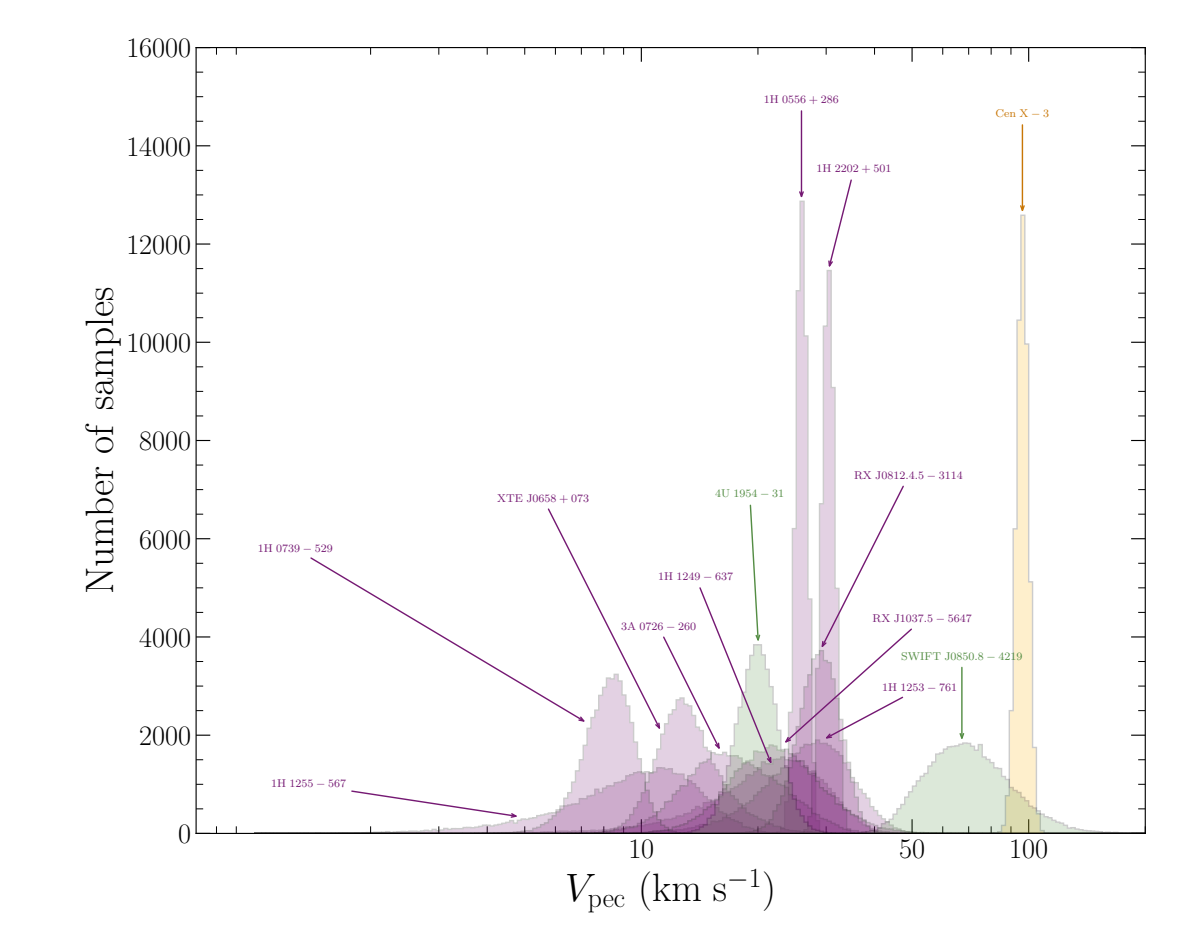**Figure 14.** Individual probability distributions of $V_{\rm pec}$ for RLOs (yellow), SyXRBs (green) and unclear classes (margenta). Systems with assumed $V_{\rm r}$ values using isotropic assumption are included here. For each source, 50,000 random samples are drawn.

not to adopt this $V_{\rm r}$ value. Instead, we employ our ansatz approach of computing an isotropic estimate of $V_{\rm pec}$, resulting in a substantially lower $V_{\rm pec,3D}^{\rm iso}$ of 10.4 km s^{-1}. With this assumption, the source comfortably aligns with the BeXRB sub-group, consistent with the typical velocities for other in BeXRB sub-group.

This paper has been typeset from a TEX/LATEX file prepared by the author.